Higgs funnel region of supersymmetric dark matter for small $\tan\beta$ and renormalization group effects on pseudoscalar Higgs boson with scalar mass nonuniversality

Utpal Chattopadhyay and Debottam Das*

Department of Theoretical Physics, Indian Association for the Cultivation of Science, 2A and 2B Raja S.C. Mullick Road, Jadavpur, Kolkata 700 032, India

(Received 13 October 2008; published 10 February 2009)

A nonuniversal scalar mass supergravity type of model is explored where the first two generations of scalars and the third generation of sleptons may be very massive. The lighter or vanishing third generation of squarks as well as Higgs scalars at the unification scale cause the radiative electroweak symmetry breaking constraint to be less prohibitive. Thus, both flavor-changing neutral-current/*CP*-violation problems as well as the naturalness problem are within control. We identify a large slepton mass effect in the renormalization group equations of $m_{H_D}^2$ (for the down type of Higgs) that may turn the latter negative at the electroweak scale even for a small $\tan\beta$. A hyperbolic branch/focus pointlike effect is found for m_A^2 that may result in very light Higgs spectra. The lightest stable particle is dominantly a b-ino that pair annihilates via Higgs exchange, giving rise to a Wilkinson Microwave Anisotropy Probe satisfied relic density region for all $\tan\beta$. Detection prospects of such lightest stable particles in the upcoming dark matter experiments both of direct and indirect types (photon flux) are interesting. The Higgs bosons and the third generation of squarks are light in this scenario and these may be easily probed besides charginos and neutralinos in the early runs of the Large Hadron Collider.

DOI: 10.1103/PhysRevD.79.035007 PACS numbers: 04.65.+e, 13.40.Em, 13.85.−t, 14.60.Ef

I. INTRODUCTION

Low energy supersymmetry (SUSY) [1] is one of the most active fields of research for physics beyond the standard model (SM) [2]. A minimal extension of the standard model when supersymmetry is incorporated is the minimal supersymmetric standard model (MSSM) [1,3] that includes two Higgs doublets. The model, however, has a large number of SUSY breaking parameters and this motivates one into studying models with specific mechanisms for breaking SUSY. The latter involves high scale physics input and renormalization group analyses. This in general leads to a large reduction of the number of unknown parameters. The minimal supergravity (mSUGRA) [4] model is one of the well-studied SUSY models. It requires very few input parameters at the gauge coupling unification scale or grand unified theory (GUT) scale, $M_G \simeq 2 \times 10^{16}$ GeV. The parameters indeed quantify our ignorance of the exact nature of SUSY breaking. The model incorporates the radiative breaking of electroweak symmetry (REWSB). The unification scale universal input parameters are: (i) the gaugino mass parameter $m_{1/2}$, (ii) the scalar mass parameter m_0, and (iii) the trilinear SUSY breaking parameter A_0. Additionally, one has to provide with $\tan\beta$, the ratio of Higgs vacuum expectation values and the sign of the Higgsino mixing parameter μ. Renormalization group evolutions are used to obtain the electroweak scale parameters of MSSM.

There is, however, no *a priori* necessity of considering such universalities of parameters. Indeed, it is worthwhile to explore scenarios with nonuniversalities in the scalar or in the gaugino masses at the unification scale [5–11]. Nonuniversal scalar masses may appear because of nonflat Kähler potential [12]. However, one must be careful to accommodate the stringent constraints from phenomena involving flavor changing neutral currents (FCNC). Satisfying FCNC constraints demands near degeneracy of the first two generations of scalar masses but the requirements on the third generation of scalars as well as the Higgs scalars are not so stringent [13,14]. Thus it is seen that FCNC constraints as well as constraints from *CP*-violating phases (for example, those arising from the electric dipole moments of the electron and neutron) may be managed by introducing multi-TeV scalar masses for the first two generations of scalars [15]. The third generation of scalar masses and the Higgs scalar masses, however, should be adequately light in order to satisfy naturalness [16]. There have been several efforts for obtaining the desired features as outlined above. Analyses with radiatively generated inverted mass hierarchy models (RIMH) were made in Refs. [14,17,18]. In Ref. [18] the authors achieved the above-mentioned requirements at the electroweak scale by using $t - b - \tau$ Yukawa unification with a special nonuniversal relationship among the scalar masses at M_G. Here, the Higgs and the third generation of scalar masses are rapidly diminished at the electroweak scale via RG evolutions. However, the Yukawa unification and the consideration of REWSB constrain such models heavily. A second realization of the above idea is partially possible via the hyperbolic branch (HB)/focus point (FP) [19,20] scenarios where the scalars may become considerably massive (multi-TeV) in a subset of the typical mSUGRA parameter space satisfying universal boundary conditions while fine-

*tpuc@iacs.res.in; tpdd@iacs.res.in

tuning [16] still remains small. A third possibility was considered in Ref. [21], where plain decoupling arguments motivated the authors in using explicit splitting at M_G between the scalars belonging to the first two generations and the same of the third generation (along with the Higgs scalars). Here the first two generations of scalars were chosen in the multi-TeV domain whereas the third generation of scalars as well as the Higgs scalars were considered to be in the sub-TeV zone. Additionally, a large value of the trilinear coupling parameter was chosen in Ref. [21] for the first two generations. Universality of scalar masses in the first two generations along with a choice of a different scalar mass parameter for the third generation as well as the Higgs scalars, or even splitting of squarks and sleptons within the third generation itself, have also been considered in Refs. [22–24]. In Ref. [23] the authors additionally considered nonuniversality in the gaugino masses and analyzed the fine-tuning aspect of computing the relic density of dark matter in addition to obtaining a parameter zone of the MSSM corresponding to a well-tempered neutralino [25]. Similarly, analyses with only nonuniversalities in the Higgs scalar may be seen in Refs. [6,8,10,26]. A comprehensive set of characteristic possibilities for varieties of nonuniversal SUGRA scenarios may be seen in Ref. [27].

In this analysis we explore a SUGRA scenario with nonuniversal scalar masses that (i) allows to have very large first two generations of scalar masses so as to obey the FCNC and the *CP*-violation limits easily (i.e. without requiring any ultrasmall phases) and that would not impose any additional price on fine-tuning, (ii) spans a large amount of MSSM parameter space satisfying the neutralino relic density constraint from WMAP data by not requiring any delicate mixing of *b*-ino and Higgsinos, so that we would find a *b*-ino-dominated lightest neutralino for most of the parameter space, and (iii) satisfies the Higgs mass lower bound from LEP2 data as well as other low energy constraints. Certainly, a model with REWSB and universal scalar mass like mSUGRA is not friendly to achieve these objectives if we consider a common gaugino mass parameter below a TeV or so. The above phenomenologically inspired requirements in combination motivate us to introduce nonuniversality between the third and the first two generations of scalars as well as the Higgs scalars. This has to be such that the REWSB conditions would not become prohibitive to have a multi-TeV first two generations of scalars. Here we would like to point out that we would not be able to satisfy the mentioned objectives by considering nonuniversalities only in the Higgs scalar masses.

A simpler and purely phenomenological attempt in this direction in a universal gaugino mass framework could be to generate all the third generation of scalar masses and the Higgs scalar masses radiatively, starting from zero values at the unification scale, while keeping the first two generations of scalar masses universal (and this may be in the multi-TeV zone). We point out that starting with a similar range of values for the Higgs scalars as with the third generation of scalars at M_G would be desirable since this would lead to a similar range of mass values for all the soft-SUSY breaking terms contributing to REWSB after RG evolutions. However, if we consider all the third generation of scalars at M_G to be light, we would find stau ($\tilde{\tau}$) becoming the lightest stable particle (LSP) or even tachyonic at the electroweak scale. On a similar note, we remind that such an appearance of tachyonic sleptons also arise in the anomaly mediated supersymmetry breaking (AMSB) analyses, and it is avoided purely by a phenomenologically inspired way of adding an appropriate nonzero mass value to all the scalars at the unification scale in the minimal AMSB scenario [28]. Thus with a simple motivation of managing with FCNC and *CP* violation, naturalness as well as the dark matter constraints concurrently we consider a nonzero mass value for the third generation of sleptons, while having the masses of squarks of the third generation and the Higgs scalars vanishing at M_G. Additionally, for convenience we set the third generation of slepton mass parameters the same as that of the first two generations of scalars at M_G.

Thus, the parameters of our nonuniversal scalar mass model which will henceforth be called the NUSM model is given by

$$\tan\beta,\ m_{1/2},\ A_0,\ \mathrm{sign}(\mu), \quad \text{and} \quad m_0, \tag{1}$$

where the scalar mass input assignments at M_G are as follows: (i) The unification scale mass parameter for the first two generations of squarks, sleptons, and the third generation of sleptons is m_0, where m_0 is allowed to span up to a very large value. (ii) The mass parameters for the third generation of squarks and Higgs scalars are set to zero. We could have also chosen a nonvanishing value for (ii) as long as it is sufficiently small. We may note here that different values of mass parameters for squarks and sleptons at M_G may appear in orbifold models with large threshold corrections. This is related to having different modular weights associated with the squarks and the sleptons in a given generation [29,30].

As we will see below, the NUSM model provides with a highly *b*-ino-dominated neutralino dark matter over almost its full range of parameter space. It has an interesting feature of having a large funnel region, a region of parameter space where the associated annihilation channels are characterized by the direct-channel pole $2m_{\tilde{\chi}_1^0} \simeq m_A,\ m_H$. We note that unlike mSUGRA where one finds the funnel region only for a large value of $\tan\beta$, here in the NUSM one finds it for almost all possible values of $\tan\beta(\gtrsim 5)$. We will also see that the NUSM is further characterized by a lighter m_A or m_H particularly when m_0 is large and this is found even for small values of $\tan\beta(\sim 10)$. A small part of the parameter space may be far from the decoupling [31]

region of Higgs boson mixing that causes the lighter CP-even Higgs boson (h-boson) to be non-standard model-like [32]. This in turn reduces the lower bound of m_h much below the LEP2 Higgs boson mass limit.

In this work we include a semianalytic calculation that first points out a large mass effect in the solution of the renormalization group equations (RGE) of $m_{H_D}^2$. The effect causes a hyperbolic branch/focus point-like behavior[1] in $m_A^2 (\simeq m_{H_D}^2 - m_{H_U}^2)$ that may cause m_A to become smaller even for a small $\tan\beta$ as mentioned above. Here we remind that m_A typically becomes smaller in mSUGRA only for large $\tan\beta$.

The paper is organized as follows. In Sec. II we will primarily discuss the large mass RGE effects in the NUSM on m_A^2 and its consequent reduction for large m_0 via a HB/FP-like effect. We will obtain the semianalytic results which will also be verified by numerical computation. In Sec. III we will study the cold dark matter constraint from Wilkinson Microwave Anisotropy Probe (WMAP) data including also the constraints from the LEP2 Higgs bound, $b \to s + \gamma$, and $B_s \to \mu^+ \mu^-$. We will also discuss a few sample points in the context of the Large Hadron Collider (LHC) reach. In Sec. IV we will discuss the direct and indirect detection (via continuous gamma ray) rates of the LSP. Finally, we will conclude in Sec. V.

II. THE NONUNIVERSAL SCALAR SCENARIO: NUSM

In this section we focus on the key elements that are important for the NUSM. The primary quantities of phenomenological interest are μ and m_A. These in turn have important significance on the following: (i) the issue of fine-tuning, ii) the presence of non-standard model-like lighter Higgs boson mass bound for a limited region of parameter space, (iii) dark matter, and (iv) collider discovery possibilities. Additionally, we remind ourselves about obtaining a lighter third generation of squarks at the electroweak scale and this is of course related to their vanishing values at the unification scale.

To start with we write down the REWSB results,

$$\mu^2 = -\frac{1}{2}M_Z^2 + \frac{m_{H_D}^2 - m_{H_U}^2 \tan^2\beta}{\tan^2\beta - 1} + \frac{\Sigma_1 - \Sigma_2 \tan^2\beta}{\tan^2\beta - 1}, \tag{2}$$

and

$$\sin 2\beta = 2B\mu/(m_{H_D}^2 + m_{H_U}^2 + 2\mu^2 + \Sigma_1 + \Sigma_2), \tag{3}$$

[1]We remind that the well-known HB/FP effect that occurs in $m_{H_U}^2$ is associated with the first minimization condition of radiative electroweak symmetry breaking. In this analysis we do not have such an effect. On the contrary we have a similar HB/FP effect for small values of $\tan\beta$ in connection with the second minimization condition that is associated with m_A^2.

where $\Sigma_{1,2}$ represents the one-loop corrections [33,34] that become small in the scale where the Higgs potential $V_{\rm Higgs}$ is minimized. We may approximately consider $\mu^2 \simeq -m_{H_U}^2$ (for $\tan\beta \gtrsim 5$) and $m_A^2 = m_{H_D}^2 + m_{H_U}^2 + 2\mu^2 \simeq m_{H_D}^2 - m_{H_U}^2$ at tree level.

The associated one-loop RGEs are given by (neglecting the very small first two generations of Yukawa contributions),

$$\frac{dm_{H_D}^2}{dt} = \left(3\tilde{\alpha}_2 \tilde{m}_2^2 + \frac{3}{5}\tilde{\alpha}_1 \tilde{m}_1^2\right) - 3Y_b(m_{H_D}^2 + m_Q^2 + m_D^2 + A_b^2) - Y_\tau(m_{H_D}^2 + m_L^2 + m_E^2 + A_\tau^2) + \frac{3}{10}\tilde{\alpha}_1 S_0, \tag{4}$$

$$\frac{dm_{H_U}^2}{dt} = \left(3\tilde{\alpha}_2 \tilde{m}_2^2 + \frac{3}{5}\tilde{\alpha}_1 \tilde{m}_1^2\right) - 3Y_t(m_{H_U}^2 + m_Q^2 + m_U^2 + A_t^2) - \frac{3}{10}\tilde{\alpha}_1 S_0. \tag{5}$$

Here we have $t = \ln(M_G^2/Q^2)$ with Q being the renormalization scale. $\tilde{\alpha}_i = \alpha_i/(4\pi)$ for $i = 1, 2, 3$ are the scaled gauge coupling constants (with $\alpha_1 = \frac{5}{3}\alpha_Y$) and $\tilde{m}_i$ are the running gaugino masses, where $i = 1, 2, 3$ refers to U(1), SU(2), and SU(3) gauge groups, respectively. Y_j represents the scaled and squared Yukawa couplings, e.g., $Y_j \equiv h_j^2/(4\pi)^2$ where h_j is a Yukawa coupling ($j = 1, 2, 3$ stands for t, b, τ, respectively). The quantity S_0 which is shown below may become relevant for a general set of nonuniversal boundary condition for scalars. However, in this analysis it is zero at M_G and it causes only a negligible effect,

$$S_0 = m_{H_U}^2 - m_{H_D}^2 + \Sigma_k(m_{q_k}^2 + m_{d_k}^2 + m_{e_k}^2 - m_{l_k}^2 - 2m_{\tilde{u}_k}^2) + (m_Q^2 + m_D^2 + m_E^2 - m_L^2 - 2m_U^2), \tag{6}$$

where the subscript k for $k = 1$ or 2 indicates the first two generations.

The solutions for μ^2 and m_A^2 valid up to a moderately large value of $\tan\beta$ (10 or so) follow from Ref. [6] after appropriately considering the NUSM parameters. This involves ignoring h_b and h_τ in the limit of a small $\tan\beta$. The solutions read

$$\mu^2 = m_0^2 C_1 + A_0^2 C_2 + m_{1/2}^2 C_3 + m_{1/2} A_0 C_4 - \frac{1}{2}M_Z^2 + \frac{3}{5}\frac{\tan^2\beta + 1}{\tan^2\beta - 1}S_0 p, \tag{7}$$

and

$$m_A^2 = m_0^2 D_1 + A_0^2 D_2 + m_{1/2}^2 D_3 + m_{1/2} A_0 D_4 - \frac{1}{2}M_Z^2 + \frac{6}{5}\frac{\tan^2\beta + 1}{\tan^2\beta - 1}S_0 p. \tag{8}$$

Here p is given by $p = \frac{5}{66}[1 - (\frac{\tilde{\alpha}_1(t)}{\tilde{\alpha}_1(0)})]$. The unification

scale conditions for scalar mass squares for the NUSM may be given as $m_i^2 = (1+\delta_i)m_0^2$. Here, the subscript i for δ_i stands for: $i \equiv H_D, H_U, Q_L, u_R, d_R, l_L, e_R$. For NUSM one has $\delta_{H_u} = \delta_{H_D} = \delta_{Q_L} = \delta_{u_R} = \delta_{d_R} = -1$ and $\delta_{l_L} = \delta_{e_R} = 0$. These unification scale conditions allow us to define a quantity δ that appears in the expressions of the coefficients C_1 and D_1 as shown below. It follows that $\delta = -1$ for the NUSM and $\delta = 0$ for mSUGRA. We note that only C_1 among C_i's and D_1 among D_i's depend on δ and one obtains,[2]

$$C_1 = (1+\delta)\frac{1}{\tan^2\beta - 1}\left(1 - \frac{3D_0 - 1}{2}\tan^2\beta\right), \quad \text{and}$$
$$D_1 = \frac{3}{2}(1+\delta)\frac{\tan^2\beta + 1}{\tan^2\beta - 1}(1 - D_0). \tag{9}$$

Here, $D_0 \simeq 1 - (m_t/200\sin\beta)^2 \lesssim 0.2$. The definitions of the quantities C_i and D_i for $i \neq 1$ may be seen in the appendix. As mentioned above, for the NUSM one has $\delta = -1$. Hence, Eqs. (7)–(9) show that at the level of approximation where h_b and h_τ are ignored, μ^2 and m_A^2 are independent of m_0. We will, however, see that both μ^2 and m_A^2 would actually depend on m_0. While the dependence of μ^2 on m_0 would be caused by two-loop RGE effects in $m_{H_U}^2$, the same for m_A^2 is very prominent even at the one-loop level of RGE and this is found when we include the effects due to h_b and h_τ which are especially important for the NUSM. The following subsection describes our improved results.

Large slepton mass RGE effect on pseudoscalar Higgs boson—a hyperbolic branch/focus point-like effect in m_A^2 for small $\tan\beta$

Numerical computation shows that unlike what is seen from Eqs. (8) and (9), m_A^2 may indeed decrease very rapidly with an increase of m_0 for large values of the latter. There are two reasons behind the above behavior: (i) the choice of vanishing Higgs scalars in the NUSM at the unification scale M_G and (ii) a large slepton mass (LSM) effect in the RGE of Eq. (4) via the tau-Yukawa term. Henceforth, we will refer the combined effect of (i) and (ii) as the LSM effect. In this analysis we first compute $m_{H_D}^2$ analytically without ignoring the terms involving h_b and h_τ. The calculation essentially keeps the terms involving the bottom and the tau-Yukawa couplings similar to what was used for the top-Yukawa term of Eq. (4) in Refs. [6,35]. This results in

$$m_{H_D}^2 = C_{H_D} m_0^2 + m_{1/2}^2 g(t) + \tfrac{3}{5} S_0 p. \tag{10}$$

Here $g(t)$ is a function of $\tan\beta$ [35]. The term involving S_0 vanishes in the NUSM. At the level of approximation where the bottom and tau Yukawa couplings are straightway ignored in Eq. (4), C_{H_D} would become zero in the NUSM. The result of our computation of C_{H_D} that leads to a nonvanishing value is given below:

$$C_{H_D} = C_{H_D}(U) + C_{H_D}(NU), \tag{11}$$

where

$$C_{H_D}(U) = 1 - 3(3I_2 + I_3),$$
$$C_{H_D}(NU) = \delta_{H_D} - 3I_2(\delta_{Q_L} + \delta_{d_R} + \delta_{H_D}) - I_3(\delta_{l_L} + \delta_{e_R} + \delta_{H_D}). \tag{12}$$

The quantities I_2 and I_3 are functions of $Y_i = \frac{h_i^2}{(4\pi)^2}$ for $i = 2, 3$ (b, τ). Small $\tan\beta$ solutions of Y_is, computed at the electroweak scale [35] are shown in the appendix. I_2 and I_3 defined below are computed numerically:

$$I_2 = \int_0^t Y_2(t')dt', \qquad I_3 = \int_0^t Y_3(t')dt'. \tag{13}$$

Here $t = \ln(M_G^2/M_Z^2)$. One finds $I_2,\ I_3 \ll 1$. For the NUSM, the above reduces to

$$C_{H_D} = -2I_3. \tag{14}$$

Since I_3 is proportional to the square of the τ-Yukawa coupling h_τ where $h_\tau \propto \frac{1}{\cos\beta}$, we find $|C_{H_D}|$ to be an increasing function of $\tan\beta$. For $\tan\beta = 10$, we find $C_{H_D} \simeq -0.007$. The above clearly shows the large slepton mass effect because the dependence of C_{H_D} or $m_{H_D}^2$ on I_3 arises from the term of Eq. (4) that is associated with h_τ^2. Thus with the NUSM parameters, the scalar mass term that appears as the first term in Eq. (10) is essentially contributed by the third generation of slepton masses. Equations (10) and (14) clearly show that even with a small $\tan\beta$, larger values of m_0 may reduce $m_{H_D}^2$ appreciably and may turn the latter negative. This demonstrates the LSM effect as mentioned before.[3] We are not aware of any past reference that pointed out this large mass effect or provided semianalytic expressions. For larger $\tan\beta$, C_{H_D} may be appreciably large and negative and causes the LSM effect to become prominent even for a smaller value of m_0.

[2] In Ref. [6] the authors considered nonuniversalities in the masses of Higgs scalars and the third generation scalars m_{Q_L} and m_{u_R}. However, the NUSM additionally requires nonuniversality in m_{d_R}.

[3] (i) We must mention that if we had chosen the values of Higgs scalar masses to be m_0 at the unification scale, the resulting coefficient of m_0^2 in $m_{H_D}^2$ would be positive and the latter would no longer be a decreasing function of m_0. (ii) We further note that the fact that the third generation of squark masses are vanishing in the NUSM also makes the LSM effect prominent. For example, had we considered nonvanishing values for m_Q and m_D ($= m_0$, i.e. $\delta_{Q_L} = \delta_{d_R} = 0$) we would find the terms in Eq. (12) that are associated with I_2 to become more prominent. This would have caused $m_{H_D}^2$ to be further negative. However, it could also cause m_Q^2 to turn tachyonic at the electroweak scale. We have also checked this fact numerically.

We note that there is no LSM effect that may modify μ^2 of Eq. (7) at the one-loop level. This is simply because $\mu^2 \simeq -m_{H_U}^2$ and there is no possibility of having a LSM effect in the corresponding RGE of Eq. (5). On the other hand, an improved $m_{H_D}^2$ as obtained above in Eqs. (10) and (14) changes the result of m_A^2 [Eqs. (8) and (9)] but the latter does not receive any additional m_0^2 dependence other than what is already contributed from Eq. (14). Thus it follows that the coefficient of m_0^2 when Eq. (8) is modified would be C_{H_D}. As a result, in the above analysis that is valid for small $\tan\beta$ below 10 or 15, we find that the LSM effect causes m_A^2 to have a HB/FP-like behavior for its dependence on m_0 and $m_{1/2}$. Hence, m_A may become significantly small for a large m_0 because of a cancellation between the terms. This of course may happen even for a small value of $\tan\beta$. A very large m_0 would cause m_A^2 to become tachyonic or would result in an absence of REWSB [Eq. (3)]. For a large $\tan\beta$ on the other hand, the LSM effect is drastically enhanced. We comment here that in spite of showing the one-loop results we performed a complete numerical solution of the RGEs up to two loops in this analysis using SUSPECT [36].

We now point out that a simple nonuniversal Higgs scalar mass scenario as described in Ref. [10] may also provide a small m_A along with a funnel type of region that satisfies the WMAP data, for a smaller value of $\tan\beta$. We emphasize, in particular, the case where nonuniversality was analyzed with a unified Higgs scalar mass in Ref. [10]. However, unlike the NUSM these scenarios are very much constrained via REWSB so that considering larger values

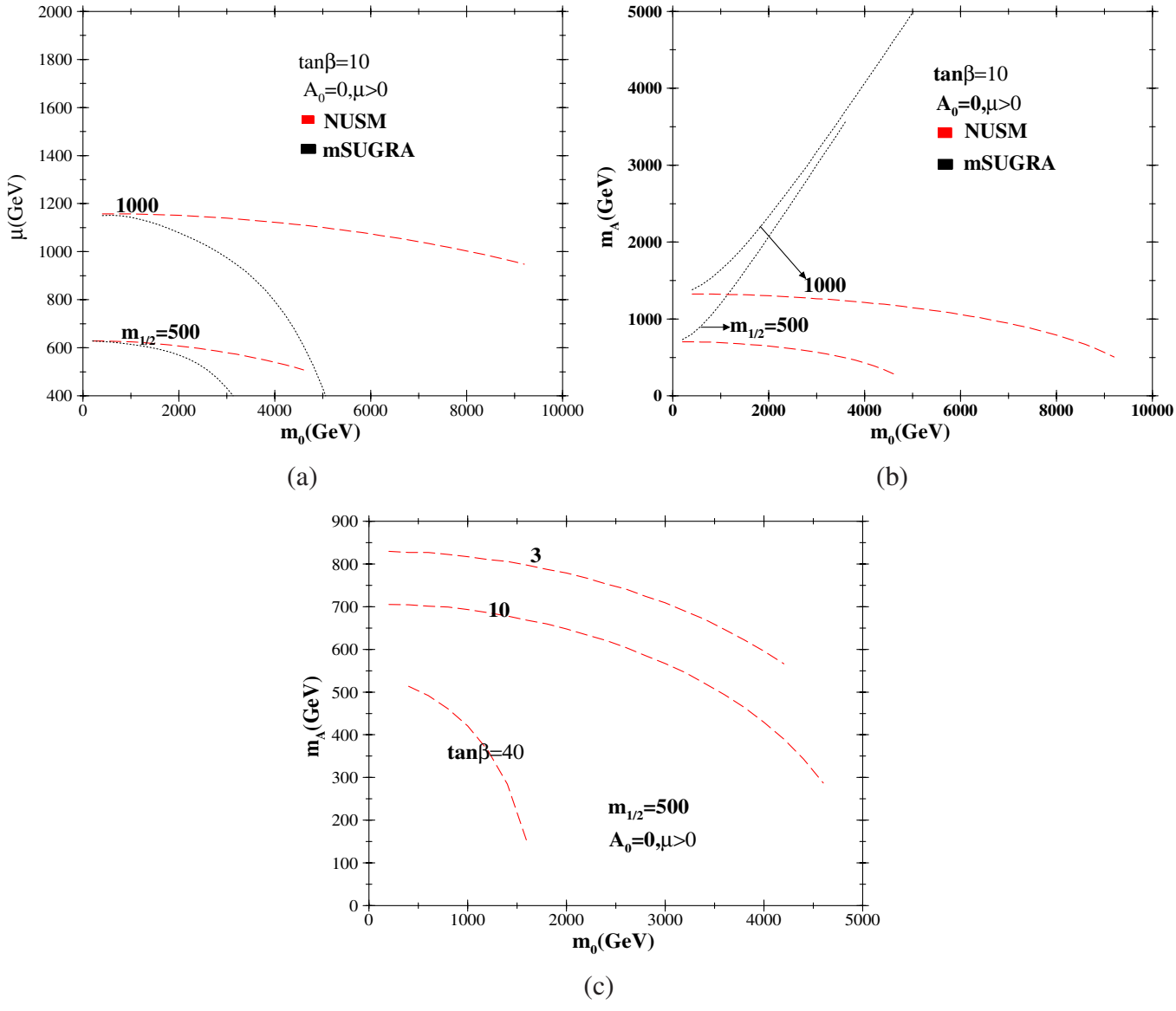

FIG. 1 (color online). (a) Variation of μ with m_0 for $\tan\beta = 10$, $A_0 = 0$, and $m_{1/2} = 500$, 1000 GeV. The red dashed lines represent the curves for the NUSM and the black dotted lines represent the same for mSUGRA. (b) Same as (a), but CP-odd Higgs (m_A) is plotted against m_0. (c) Shows the variation of m_A with m_0 in the NUSM for different values of $\tan\beta$ when $m_{1/2} = 500$ GeV.

of masses for the first two generations of scalars, an easier way to control FCNC and CP-violation effects is not possible. In these nonuniversal Higgs scalar models m_A becomes small for small values of $\tan\beta$, only when tachyonic values of $m^2_{H_D}$ and $m^2_{H_U}$ (assumed equal) are considered at the unification scale and this severely reduces the available parameter space. Additionally, one may obtain an A-pole annihilation region or a funnel region for a small value of $\tan\beta$ in the so-called sub-GUT CMSSM scenario [37].

We will now describe our results as obtained by using SUSPECT [36]. Figure 1 shows the variation of μ and m_A when m_0 is varied in the NUSM and mSUGRA. Figure 1(a) shows the effect of varying m_0 in mSUGRA and in the NUSM for $m_{1/2} = 500$ GeV and 1 TeV. A small reduction of $|\mu|$ (10 to 20%) is seen in the NUSM when m_0 is increased up to 5 or 10 TeV. The approximate one-loop result of Eq. (7) and Eq. (9) with $\delta = -1$ as in the NUSM, however, would indicate a flat μ over a variation of m_0. The figure of course shows a moderately varying μ and we have checked that this variation has its origin in two-loop RGE effects. The two different $m_{1/2}$ contours for mSUGRA, however, show a decreasing behavior of μ when m_0 is enhanced. This happens simply because of the HB/FP effect existing in mSUGRA. Figure 1(b) shows the results for m_A which have two sets of contours for $m_{1/2} = 500$ GeV and 1 TeV corresponding to mSUGRA and the NUSM. In contrast to mSUGRA where m_A rapidly increases with m_0, the behavior in the NUSM is opposite so that we may find a very light pseudoscalar Higgs boson via the LSM effect. The decrease of m_A is even more pronounced for a large value of $\tan\beta$ and this may be easily seen in Fig. 1(c) where a variation of m_A vs m_0 is shown for a given $m_{1/2}(= 500$ GeV) for three different values of $\tan\beta$. The curves end in the larger m_0 sides for a few different reasons. For $\tan\beta \lesssim 10$, the largest m_0 limit is caused by stop mass becoming very light or unphysical. On the other hand for $\tan\beta \lesssim 15$ the largest m_0 limit is given by the absence of REWSB (i.e. m^2_A turning negative).

The LSM effect may be explicitly seen in Fig. 2 where we plot squared scalar masses of Higgs scalars as well as their difference $m^2_A \simeq m^2_{H_D} - m^2_{H_U}$ with respect to a variation over the renormalization scale Q for mSUGRA and the NUSM for $\tan\beta = 10$, $m_{1/2} = 400$ GeV, and $A_0 = 0$. Figure 2(a) corresponds to mSUGRA for $m_0 = 1$ TeV whereas Fig. 2(b) shows the case of the NUSM for $m_0 = 5$ TeV. We have chosen different values of m_0 in the two figures because of the fact that a large m_0 is prohibited in mSUGRA via the REWSB constraint whereas a choice of a small m_0 in the NUSM would have a negligible LSM effect. Clearly, $m^2_{H_D}$ stays positive at the electroweak scale in mSUGRA [Fig. 2(a)]. On the other hand the same for the NUSM turns toward a negative value while running from M_G to the electroweak scale [Fig. 2(b)] and this essentially shows the LSM effect in m^2_A. Thus a typical large $\tan\beta$ phenomenon that occurs in mSUGRA is obtained in the NUSM for a small $\tan\beta$.

III. COLD DARK MATTER CONSTRAINT AND EXTENDED FUNNEL REGION

In the supergravity type of models $\tilde{\chi}^0_1$ becomes the LSP for most of the parameter space [38,39] and we assume that the cold dark matter relic density is entirely due to $\tilde{\chi}^0_1$. Considering WMAP data [40] one finds a 3σ limit as shown below:

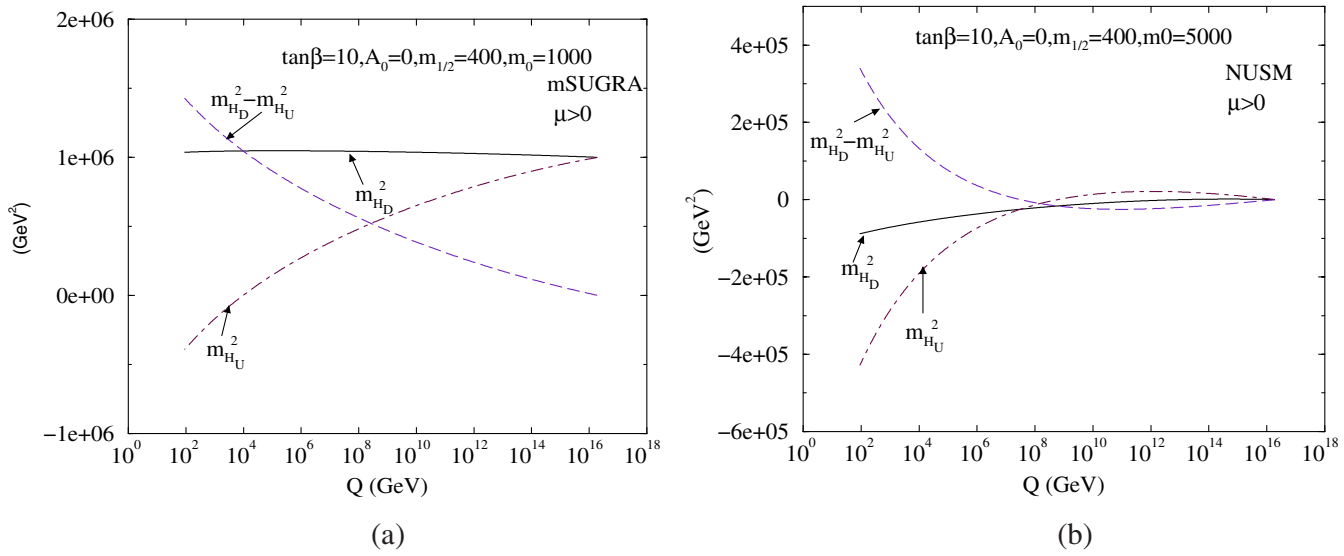

FIG. 2 (color online). (a) Variation of squared Higgs scalar masses and their difference ($\equiv m^2_A \simeq m^2_{H_D} - m^2_{H_U}$) with renormalization scale Q for $\tan\beta = 10$, $m_{1/2} = 400$ GeV, $m_0 = 1000$ GeV, and $A_0 = 0$ for mSUGRA. (b) Same as (a), except for $m_0 = 5000$ GeV and for the NUSM. $m^2_{H_D}$ turns negative via the LSM effect.

$$0.091 < \Omega_{\rm CDM} h^2 < 0.128, \tag{15}$$

where $\Omega_{\rm CDM} h^2$ is the DM relic density in units of the critical density. Here, $h = 0.71 \pm 0.026$ is the Hubble constant in units of 100 Km s^{-1} Mpc^{-1}. In the thermal description, the LSP was in thermal equilibrium with the annihilation products at a very high temperature of the early universe ($T \gg m_{\tilde{\chi}_1^0}$). The annihilation products include fermion pairs, gauge boson pairs, Higgs boson pairs, or gauge boson-Higgs boson combinations and they are produced via s, t, and u-channel processes. As the temperature decreased the annihilation rate fell below the expansion rate of the universe and the LSP went away from the thermal equilibrium and freeze-out occurred. The current value of $\Omega_{\tilde{\chi}_1^0} h^2$ is computed by solving the Boltzmann equation for $n_{\tilde{\chi}_1^0}$, the number density of the LSP in a Friedmann-Robertson-Walker universe. The above computation essentially involves finding the thermally averaged quantity $\langle \sigma_{\rm eff} v \rangle$, where v is the relative velocity between two annihilating neutralinos and $\sigma_{\rm eff}$ is the neutralino annihilation cross section that includes all the final states. In addition to annihilations one considers coannihilations [41–45] which are annihilations of the LSP with sparticles close in mass values with that of the LSP. The cross section sensitively depends on the nature of the composition of the LSP. In the MSSM, the LSP is a mixed state of b-ino ($\tilde{B}$), w-ino ($\tilde{W}$), and Higgsinos ($\tilde{H}_1^0$ $\tilde{H}_2^0$):

$$\tilde{\chi}_1^0 = N_{11}\tilde{B} + N_{12}\tilde{W}_3 + N_{13}\tilde{H}_1^0 + N_{14}\tilde{H}_2^0. \tag{16}$$

Here N_{ij} are the elements of the matrix that diagonalize the neutralino mass matrix. The gaugino fraction F_G of the lightest neutralino is defined by $F_g = |N_{11}|^2 + |N_{12}|^2$. A gauginolike LSP may be defined to have F_g very close to $1(\gtrsim 0.9)$. On the other side, a Higgsino-like LSP would have $F_g \lesssim 0.1$. For values in between, the LSP could be identified as a gaugino-Higgsino mixed state. The MSSM with gaugino masses universal at M_G has a few distinct regions in general that satisfy the WMAP constraint. In this section we point out the existence of such regions in the context of the NUSM. (i) The *bulk annihilation* region in mSUGRA is typically characterized by smaller scalar masses and smaller values of $m_{1/2}$ where the LSP is b-ino dominated. A b-ino-dominated LSP couples favorably with right-handed sleptons. Thus, the LSP pair annihilation in the bulk annihilation region occurs primarily via a t-channel sfermion in mSUGRA. There are two important constraints that disfavor the bulk region in mSUGRA. These are the constraints (a) from the slepton mass lower limit from LEP2 [46] and (b) from the lower limit of Higgs boson mass m_h of 114.4 GeV [47].[4] (ii) The *focus point* [19] or the *hyperbolic branch* [20] region of mSUGRA is typically characterized by a small $|\mu|$ region that is close to the boundary of the lighter chargino mass lower bound. Because of a small $|\mu|$ here the LSP has a significant amount of the Higgsino component or it can even be almost a pure Higgsino.[5] Additionally the lighter chargino $\tilde{\chi}_1^\pm$ becomes lighter and coannihilations [43,44] with the LSP reduce the relic density to an acceptable level. The HB/FP region is, however, absent in the NUSM. (iii) Coannihilations of LSP may also occur with sleptons, typically staus ($\tilde{\tau}_1$) [41] in mSUGRA. These regions are associated with small $m_{1/2}$ and small m_0 zones near the boundary of the discarded zone where staus become the LSP. Stau coannihilation is also an effective way to bring the neutralino relic density to an acceptable level in the NUSM. Coannihilations of LSP may also occur with stop ($\tilde{t}_1$) in a general MSSM scenario [42] or even in mSUGRA [48]. However, in spite of having relatively lighter $\tilde{t}_1$, the NUSM does not have such a region unless one reduces the mass of $\tilde{t}_1$ further via appropriately considering nonzero values for A_0. (iv) The most important region satisfying WMAP data for our study is the Higgs-pole annihilation or *funnel* region [49,50]. The funnel region that satisfies the WMAP data is characterized by the direct-channel pole $2m_{\tilde{\chi}_1^0} \simeq m_A$, m_H. This occurs in mSUGRA typically for large $\tan\beta$ extending to larger m_0 and larger $m_{1/2}$ regions. In the NUSM, however, the funnel region occurs in all possible $\tan\beta(\gtrsim 5)$. Indeed apart from the LSP-stau coannihilation appearing in a small region, Higgs-pole annihilation is the primary mechanism in the NUSM to satisfy the WMAP constraint throughout the parameter space.

We now show the results of the computation of the neutralino relic density using the code micrOMEGAs [51]. In Fig. 3(a) that corresponds to $\tan\beta = 10$, the region with red dots in the $(m_{1/2} - m_0)$ plane satisfy the WMAP constraint [Eq. (15)] for the neutralino relic density. For a small m_0 we find the stau coannihilation region marked with red dots. The gray region below the stau coannihilation region is discarded because of the appearance of charged LSPs.

The upper gray region is discarded broadly via m_A^2 turning negative except near the boundary where there can be interplay with other constraints as described below. Thus if we concentrate on the boundary of the discarded region, the smallest $m_{1/2}$ zone (below 160 GeV or so) is ruled out by the LEP2 lower limit of sparticle masses [46]. This is followed by obtaining tachyonic sfermion scalars (particularly stop scalars) when $m_{1/2}$ is increased further up to $\simeq$ 600 GeV. The same boundary zone for the larger $m_{1/2}$ region is eliminated because of the appearance of the charge and color breaking (CCB) minima [52]. In the NUSM this happens via the CCB conditions that involve $m_{H_D}^2$, the latter becoming negative makes the CCB con-

[4]It is quite possible to have a bulk region with a nonzero A_0 [48].

[5]This holds in the inversion region of the hyperbolic branch [20].

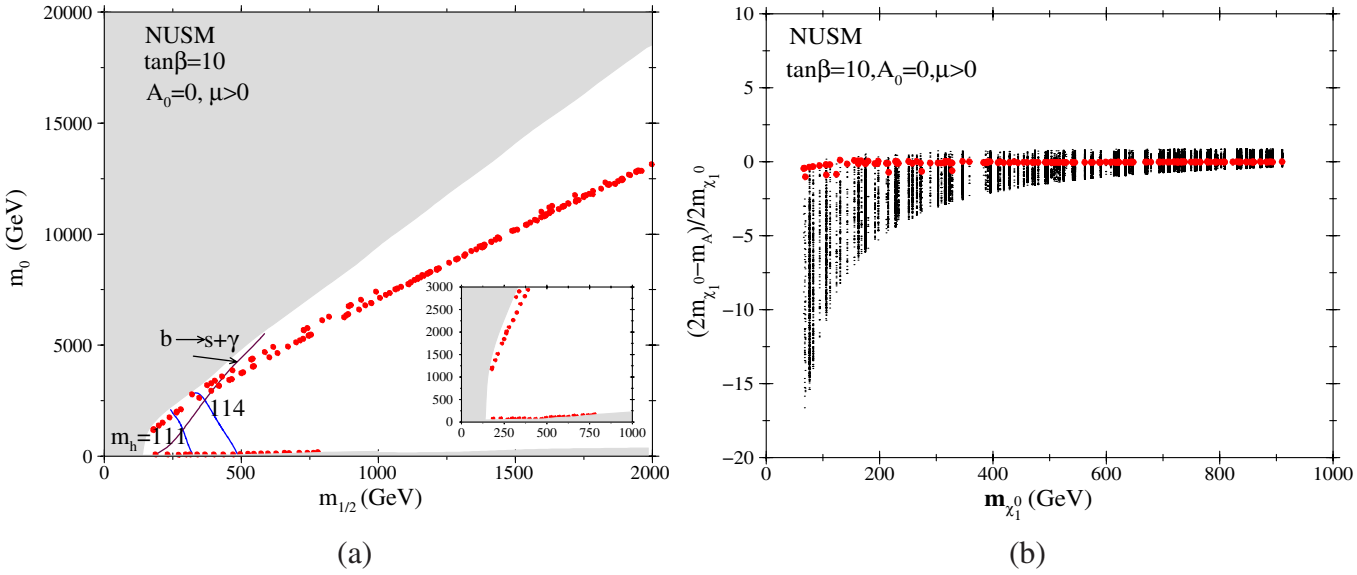

FIG. 3 (color online). (a) WMAP allowed region in the $m_{1/2} - m_0$ plane for $\tan\beta = 10$ and $A_0 = 0$ with $\mu > 0$ for the NUSM. Lighter Higgs boson mass limits are represented by solid lines. The dot-dashed line refers to the $b \to s\gamma$ limit. WMAP allowed regions are shown by red dots. The entire region is allowed via the $B_s \to \mu^+\mu^-$ bound. The small figure within the inset is shown for an improved display of the stau coannihilation zone. (b) Scattered points in the plain of $m_{\tilde{\chi}_1^0}$ vs $(2m_{\tilde{\chi}_1^0} - m_A)/2m_{\tilde{\chi}_1^0}$ shown after a scanning of $m_{1/2}$ and m_0 for $\tan\beta = 10$. Almost all the WMAP satisfied points (in red) occur near the zero of the y axis, thus suggesting the s-channel annihilation of the LSPs via A and H bosons.

straint stronger. In the region between the stau coannihilation area and the upper gray shaded discarded area one finds a long red region that satisfies the WMAP constraint for $\Omega_{\tilde{\chi}_1^0}h^2$. As mentioned before, the reason for satisfying the WMAP data is the direct-channel annihilation of two LSPs via neutral Higgs bosons. Figure 3(b) shows a scanned output for $\tan\beta = 10$ when m_0 is varied as in Fig. 3(a). The LSP mass is plotted against $(2m_{\tilde{\chi}_1^0} - m_A)/2m_{\tilde{\chi}_1^0}$ so as to show the extent of the A annihilation or funnel effect. Clearly the WMAP satisfied points shown in red fall around the zero of the y axis confirming that the funnel region appears in the NUSM for small $\tan\beta$ as well. We note that the A width can be quite large ($\Gamma_A \sim$ 10–50 GeV) and $2m_{\tilde{\chi}_1^0}$ can be appreciably away from the exact resonance zone still giving an s-channel annihilation consistent with the WMAP data. The heavy scalar Higgs boson H also significantly contributes to the total annihilation cross section. We now discuss the result of using a few constraints. First, we use the LEP2 limit [47] of 114.4 GeV for the SM Higgs boson. For the CP-even lighter SUSY Higgs boson mass m_h we use the same constraint as long as we are in the decoupling region [31] where the SUSY h boson is SM-like. In the NUSM this is true for almost all the parameter space except a very small region with small $m_{1/2}$ and for $\tan\beta \gtrsim 15$ which we will discuss later. Additionally, we note that there is an uncertainty of about 3 GeV in computing the mass of the light Higgs boson [53]. This theoretical uncertainty primarily originates from momentum-independent as well as momentum-dependent two-loop corrections, higher loop corrections from the top-stop sector, etc. Hence, we have drawn a contour for $m_h = 111$ GeV in order to consider an effective lower limit.[6]

We have further drawn the $b \to s\gamma$ contour by considering a 3σ limit [54],

$$2.77 \times 10^{-4} < \mathrm{Br}(b \to s\gamma) < 4.33 \times 10^{-4}. \qquad (17)$$

Clearly in Fig. 3(a) this constraint would keep the $m_{1/2} >$ 425 GeV region alive and this is indeed the region of super-large $m_0 \gtrsim 4$ TeV that satisfies the WMAP data. In this context we should, however, note that the $b \to s + \gamma$ constraint may be of less importance if some additional theoretical assumptions are taken into consideration. The computation of the constraint in models like mSUGRA assumes a perfect alignment of the squark and quark mass matrices. The above perfect alignment is indeed associated with an unaltered set of mixing angle factors than the Cabibbo-Kobayashi-Maskawa (CKM) factors at the corresponding SM vertices. Even a small set of off-diagonal terms in squark mass matrices at the unification scale may cause a drastic change in the mixing pattern of the squark sector at the electroweak scale. This, however, does not cause any effective change in the sparticle mass spectra or in the flavor conserving process of neutralino annihilation

[6]The following values of top and bottom quarks are considered in the SUSPECT code used in our analysis: $m_t = 172.7$ GeV and $m_b^{MS}(m_b) = 4.25$ GeV.

or in generating events in a hadron collider in any significant way. A brief review of the model-dependent assumptions for the $b \to s\gamma$ analyses may be seen in Refs. [55,56] and references therein.

We now explain an interesting aspect of the NUSM Higgs boson as a consequence of the LSM effect. As we have seen before, m_A decreases with increasing m_0 in the NUSM. We find that with larger m_0, m_A may become very light for the small $m_{1/2}$ zone so that we may find a spectrum where $m_h \sim m_H \sim M_A$ and this indeed is a consequence of moving into the intense-coupling [32] region of Higgs bosons. This results in a change in the value of the coupling g_{ZZh} ($\propto \sin(\beta - \alpha)$), where α is the mixing angle between two neutral Higgs bosons h and H. Typically in the decoupling region $\sin(\beta - \alpha)$ stays very close to 1, but in the intense-coupling region this can be considerably small like 0.5 or lesser. This effectively reduces the lower limit of m_h to 93 GeV, a value close to m_Z. In the NUSM we obtain this effect for a small region of parameter space (small $m_{1/2}$) if $\tan\beta \gtrsim 15$. Figure 4(a) shows such a region (this may also satisfy the WMAP limits) for 200 GeV $\lesssim m_{1/2} \lesssim$ 300 GeV and this appears very close to the top gray shaded discarded zone. Figure 4(b) demonstrates the existence of a small $\sin(\beta - \alpha)$ in the NUSM as discussed above. However, with $A_0 = 0$, we will see that such a very light m_A or m_h region is almost discarded via the present limit of $B_s \to \mu^+\mu^-$. The current experimental limit for $\mathrm{Br}(B_s \to \mu^+\mu^-)$ coming from CDF [57] puts a strong constraint on the MSSM parameter space. The experimental bound is given by (at 95% C.L.)

$$\mathrm{Br}\,(B_s \to \mu^+\mu^-) < 5.8 \times 10^{-8}. \tag{18}$$

The estimate of $B_s \to \mu^+\mu^-$ [58] in the MSSM sensitively depends on the mass of the A boson ($\propto m_A^{-4}$) and on the value of $\tan\beta$ ($\propto \tan^6\beta$). $B_s \to \mu^+\mu^-$ constraint eliminates the thin region along the boundary of the REWSB in the NUSM where m_A is very light. As mentioned before, for $\tan\beta \gtrsim 15$ a part of the above region for the small $m_{1/2}$ zone has a non-standard model-like h boson.

Apart from the above constraints we would like to remind that there is no nonuniversality in the first two generations in the NUSM. This saves from the stringent FCNC violating limits such as those coming from the $K_L - K_S$ mass difference or from the $\mu \to e\gamma$ bound. The splitting of the first generation and the third generation of scalars may also cause violations of FCNC bounds, although to a lesser extent. Following Ref. [22] we see that for no violation of FCNC one would need (for equal gluino and average squark masses) $|m_{\tilde{q}}(1) - m_{\tilde{q}}(3)| \lesssim m_{\tilde{q}}^2/M_W$. Here $m_{\tilde{q}}$ refers to the average squark mass. Considering the analysis performed in Ref. [22] for different gluino masses we conclude that the results of our analysis stay in the safe zone regarding the FCNC bounds in spite of the intergenerational splitting between the squarks.

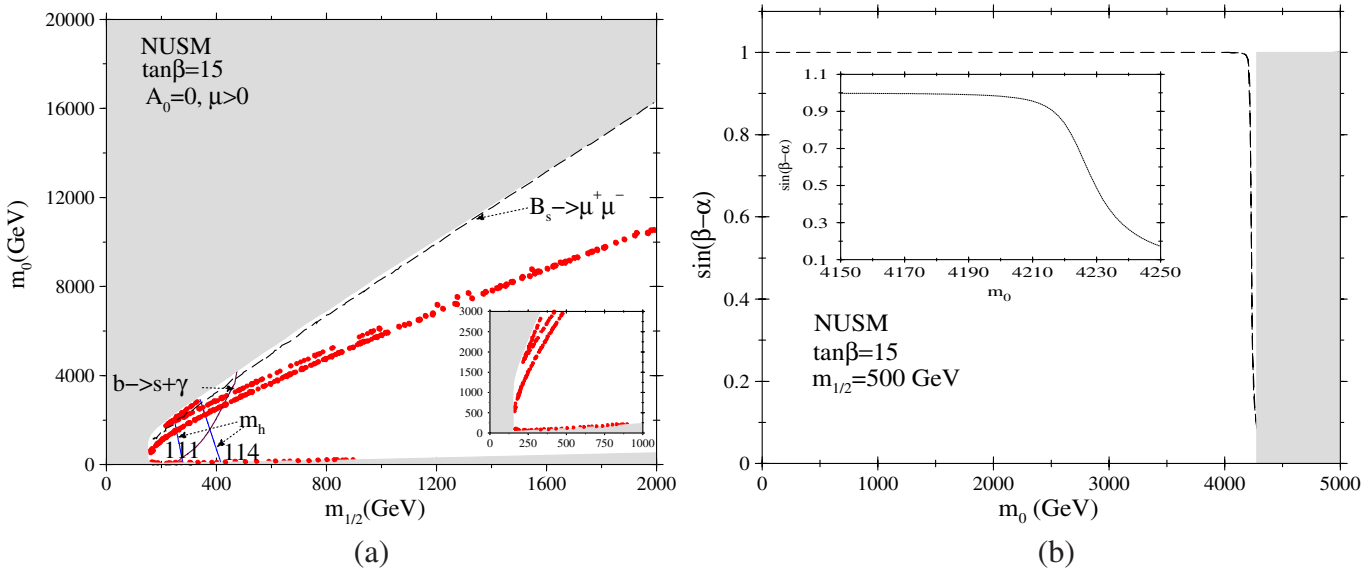

FIG. 4 (color online). (a) WMAP allowed region in the $m_{1/2} - m_0$ plane for $\tan\beta = 15$ and $A_0 = 0$ with $\mu > 0$ for the NUSM. Lighter Higgs boson mass limits are represented by solid lines. The dot-dashed line refers to the $b \to s\gamma$ limit. WMAP allowed regions are shown by red dots. The $B_s \to \mu^+\mu^-$ bound is represented by the long-dashed line and this discards a small strip of region below the discarded top gray region. The small figure within the inset is shown for an improved display of the stau coannihilation zone. (b) Variation of $\sin(\beta - \alpha)$ vs m_0 for $m_{1/2} = 500$ GeV, $\tan\beta = 15$, and $A_0 = 0$ for the NUSM. The figure shows that for large m_0, actually near the region where m_A is small, $\sin(\beta - \alpha)$ is consistently small. This is of course much away from the decoupling region of the SUSY Higgs boson. The figure in the inset shows the finer variation of $\sin(\beta - \alpha)$ within a small range of m_0. The gray shaded region refers to the similarly shaded discarded region of Fig. 4(a).

Figure 5(a) shows the results for $\tan\beta = 40$. Here the funnel region is extended up to $m_{1/2} = 1.7$ TeV. A large value of $\tan\beta$ increases h_b and h_τ and this would enhance the width Γ_A [59]. We point out that unlike Fig. 3(a), here the reach of m_0 decreases for a given $m_{1/2}$. The mass of the A boson decreases with the increase of m_0 much more rapidly because of larger h_b and h_τ arising out of larger values of $\tan\beta$. Here, the very light m_A region that satisfies the WMAP data and that evades the LEP2 Higgs boson limit exists near the top gray boundary for 250 GeV $\lesssim m_{1/2} \lesssim$ 350 GeV which is again ruled out via the $B_s \to \mu^+\mu^-$ limit. The upper gray region is typically discarded here via the REWSB constraint of m_A^2 that turns negative at the tree level. Finally, we have not imposed any limit from the muon $g-2$ data that may or may not show a discrepancy from the standard model result. It is known that using the recent $e^+ - e^-$ data leads to a 3.4σ level of discrepancy. On the other hand, using hadronic τ-decay data in computing the leading order hadronic contribution to the muon $g-2$ washes away [60] any deviation from the SM result.

Sample parameter points satisfying WMAP data for early run of LHC

We would focus on a few characteristic parameter points to discuss the nature of the NUSM spectra that satisfy the WMAP limits. Clearly one is able to reach a considerably large m_0 satisfying dark matter relic density constraints and all other necessary constraints for $m_{1/2} < 1$ TeV. As an example with $m_{1/2} = 1$ TeV, this limit is around 7 TeV for $\tan\beta = 10$, 6 TeV for $\tan\beta = 15$, and 1.6 TeV for $\tan\beta = 40$. Thus, for larger $\tan\beta$ the reach of m_0 decreases considerably. On the other hand, it is not unusual to obtain an A-pole annihilation region for a large $\tan\beta$ in popular models like mSUGRA. Hence, if we are interested in focusing on a region of the MSSM that is not available in mSUGRA type of models we would rather explore the smaller $\tan\beta$ domain of the NUSM. The other important zone of parameter space could be the region with smaller $m_{1/2}$ because this would be easily accessible in the LHC in its early run. We pick up a point on Fig. 3(a) (*scenario A*) that just satisfies the minimum value of $m_h = 111$ GeV besides being consistent with the WMAP data for cold dark matter. The input parameters are: $\tan\beta = 10$, $A_0 = 0$, $m_{1/2} = 270$ GeV, $m_0 = 2050$ GeV, and $\mathrm{sign}(\mu) = 1$. The scenario A of Table I thus has light stop and light sbottom quarks, light charginos and neutralinos, and at the same time it would have a light Higgs spectra, all of which are promising for an early LHC detection. We remind ourselves that typically the NUSM is associated with a heavy first two generations of scalars and heavy sleptons for all the three generations. We note that we have relaxed the $b \to s\gamma$ constraint keeping in mind the argument given after Eq. (17). We could of course respect the constraint, only at a price of having a little heavier spectra, still that would be very much accessible in the LHC for the third generation of squarks, Higgs bosons, charginos, etc. This, however, would not cause any essential change in the general pattern. On the other hand, with not so light m_A and with a small $\tan\beta$ the scenario A satisfies the $B_s \to \mu^+\mu^-$ limit. The *scenario B* of Fig. 4(a) refers to a special point ($\tan\beta = 15$, $A_0 = 0$, $m_{1/2} = 255$ GeV, $m_0 =$ 2000 GeV, and $\mathrm{sign}(\mu) = 1$) for which the Higgs sector is not in the decoupling region thus reducing the limit of m_h to a value near the Z-boson mass. This parameter point obeys the $B_s \to \mu^+\mu^-$ limit but as with the *scenario A* it has an inadequate $\mathrm{Br}(b \to s\gamma)$. With smaller $m_{1/2}$ and

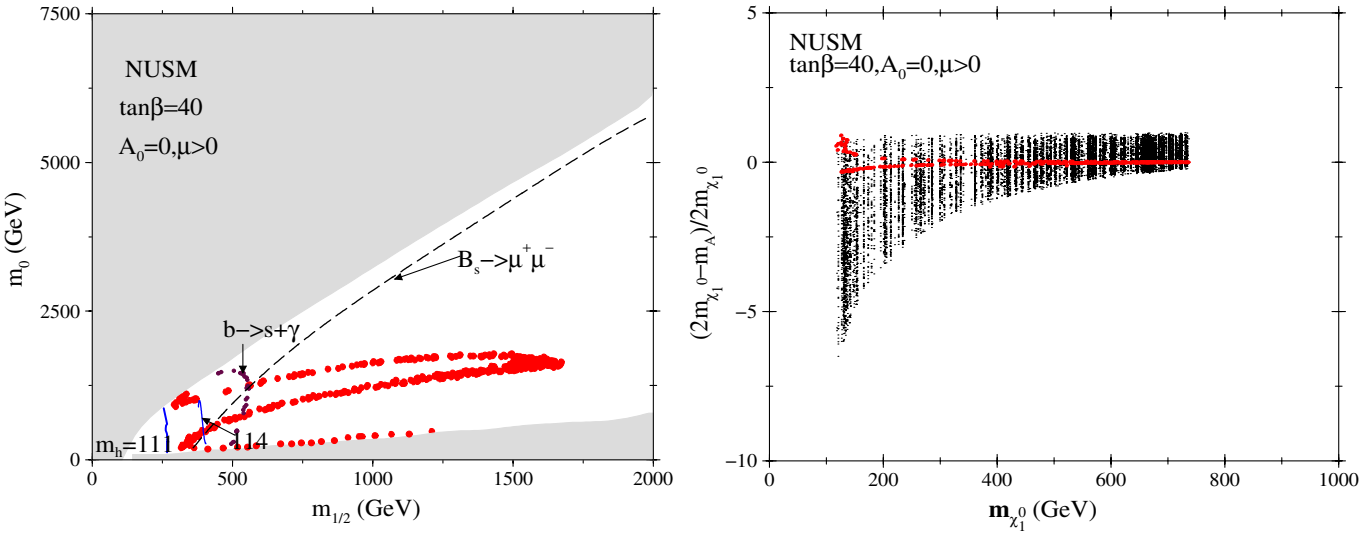

FIG. 5 (color online). Same as Fig. 3 except $\tan\beta = 40$.

TABLE I. Data for point A, B, and C. Masses are in GeV.

Parameter	A	B	C
$\tan\beta$	10.0	15.0	40.0
$m_{1/2}$	270.0	255.0	540.0
m_0	2050.0	2000.0	1250.0
A_0	0	0	0
$\mathrm{sgn}(\mu)$	1	1	1
μ	312.60	291.53	651.60
$m_{\tilde{g}}$	709.32	674.43	1278.26
$m_{\tilde{u}_L}$	2103.25	2047.68	1658.64
$m_{\tilde{t}_1}$	276.89	248.27	842.00
$m_{\tilde{t}_2}$	493.53	465.21	1028.15
$m_{\tilde{b}_1}$	390.66	354.64	958.59
$m_{\tilde{b}_2}$	434.06	403.08	1019.74
$m_{\tilde{e}_L}$	2050.19	1999.70	1296.33
$m_{\tilde{\tau}_1}$	2037.46	1972.60	1119.32
$m_{\tilde{\chi}_1^\pm}$	196.44	183.99	430.22
$m_{\tilde{\chi}_2^\pm}$	347.34	327.11	668.46
$m_{\tilde{\chi}_4^0}$	347.72	326.97	668.18
$m_{\tilde{\chi}_3^0}$	318.11	297.66	655.13
$m_{\tilde{\chi}_2^0}$	197.69	185.15	430.30
$m_{\tilde{\chi}_1^0}$	108.05	101.72	226.91
m_A	259.48	148.37	403.03
m_{H^+}	272.027	169.44	411.73
m_h	111.26	111.25	116.32
$\Omega_{\tilde{Z}_1}h^2$	0.105	0.102	0.13
$BF(b \to s\gamma)$	1.59×10^{-4}	4.65×10^{-5}	2.73×10^{-4}
$BF(B_s \to \mu^+\mu^-)$	4.02×10^{-9}	2.81×10^{-8}	5.29×10^{-8}
Δa_μ	9.31×10^{-11}	1.59×10^{-10}	6.99×10^{-10}

smaller m_0 *scenario B* has a lighter spectrum in general than *scenario A*. Particularly, we find a much smaller Higgs boson spectra. The *scenario C* (with $\tan\beta = 40$, $A_0 = 0$, $m_{1/2} = 540$ GeV, $m_0 = 1250$ GeV, and $\mathrm{sign}(\mu) = 1$), that satisfy all the constraints including the $b \to s\gamma$ bound provides a relatively heavier spectra. This is, however, still within the LHC reach for the relevant part of the NUSM as mentioned above. We note that the large m_0 domain of the NUSM is typically associated with lighter Higgs spectrum and this region may in general be probed via the production of all MSSM Higgs bosons and subsequently their decays. The squarks corresponding to the first two generations and sleptons of all the generations are large when m_0 is large. As a result the production cross section of these particles will be too low at the LHC. Thus, to see any SUSY signal for the NUSM one should primarily analyze productions and decays of gluino, stop, and sbottom in addition to charginos and neutralinos. In a part of the parameter space where the Higgs spectra is light, all the Higgs states may be produced via $pp \to h$, H, A, $H^\pm + X$ either via loop-induced processes like ($gg \to h$, H, A) or through cascade decays via heavier charginos and neutralinos $pp \to \chi_2^\pm$, χ_3^0, $\chi_4^0 \to \chi_1^\pm$, χ_2^0, $\chi_1^0 + h$, H, A, $H^\pm$. The latter decays are only allowed if enough phase space is available.

IV. DIRECT AND INDIRECT DETECTIONS OF DARK MATTER

A. Direct detection rates

We will now discuss the prospects of direct and indirect detections [61] of the neutralino (LSP) as a candidate for dark matter in the NUSM. First, we will discuss the direct detection of the LSP via measurements of nuclear recoil. Neutralinos interact via spin-independent (scalar) and spin-dependent interaction [38,62] with nucleons. The scalar cross section may be expressed in terms of the number of protons and neutrons, Z and $(A - Z)$, respectively [38], as follows:

$$\sigma_{\mathrm{scalar}} = 4\frac{m_r^2}{\pi}[Zf_p + (A - Z)f_n]^2, \tag{19}$$

where m_r is the reduced LSP mass. The quantities f_p and f_n contain all the information of short distance physics and nuclear partonic strengths and these may be seen in Refs. [63]. We will now comment on the relative strengths of spin-independent and spin-dependent neutralino-nuclear cross sections. While σ_{scalar} depends on Z and $A - Z$ quadratically, the spin-dependent interaction cross section on the other hand is proportional to $J(J + 1)$ where J is the total nuclear spin [38]. Typically the spin-independent neutralino-nucleon scattering cross sections (where $\sigma_{\chi p,\mathrm{SI}} \simeq \sigma_{\chi n,\mathrm{SI}}$) are appreciably smaller than the corresponding spin-dependent cross sections ($\sigma_{\chi p,\mathrm{SD}} \simeq \sigma_{\chi n,\mathrm{SD}}$). However, considering the fact that $\sigma_{\mathrm{SD}} \propto J(J + 1)$ and $\sigma_{\mathrm{SI}} \propto Z^2$, $(A - Z)^2$, σ_{scalar} becomes considerably larger for moderately heavy elements ($A > 30$) [3,64] like Ge, Xe, etc. But we should keep in mind that there exists some cases where σ_{SD} may become considerably larger than σ_{SI} even for $A > 30$.

The cross section σ_{scalar} mainly involves the computation of $\chi - q$ and $\chi - \tilde{g}$ scattering amplitudes. The scalar cross section at tree level is composed of t-channel Higgs boson exchange and s-channel squark exchange contributions. On the other hand, the spin-dependent cross section depends on t-channel Z exchange and s-channel squark exchange diagrams. In this analysis we compute the spin-independent cross section $\sigma_{\mathrm{scalar}}(\tilde{\chi} - p)$ for two values of $\tan\beta$ (10 and 40) for $A_0 = 0$ and $\mu > 0$ using DARKSUSY [65]. Figure 6 shows $\sigma_{\mathrm{scalar}}(\tilde{\chi} - p)$ vs $m_{\tilde{\chi}_1^0}$ for $\tan\beta = 10$ and 40 when $m_{1/2}$ and m_0 are varied as in Figs. 3 and 5, respectively. The WMAP satisfied points are shown in small (maroon) circles. We have shown the limits from CDMS (Ge) 2005 [66], XENON-10 [67], and from future experiments like SuperCDMS (Snolab) [68] and XENON1T [69]. The neutralinos with higher mass (up to 400 GeV) will be partially probed in XENON-1T while the light LSP region for $\tan\beta = 40$ is already ruled out by XENON-10 data.

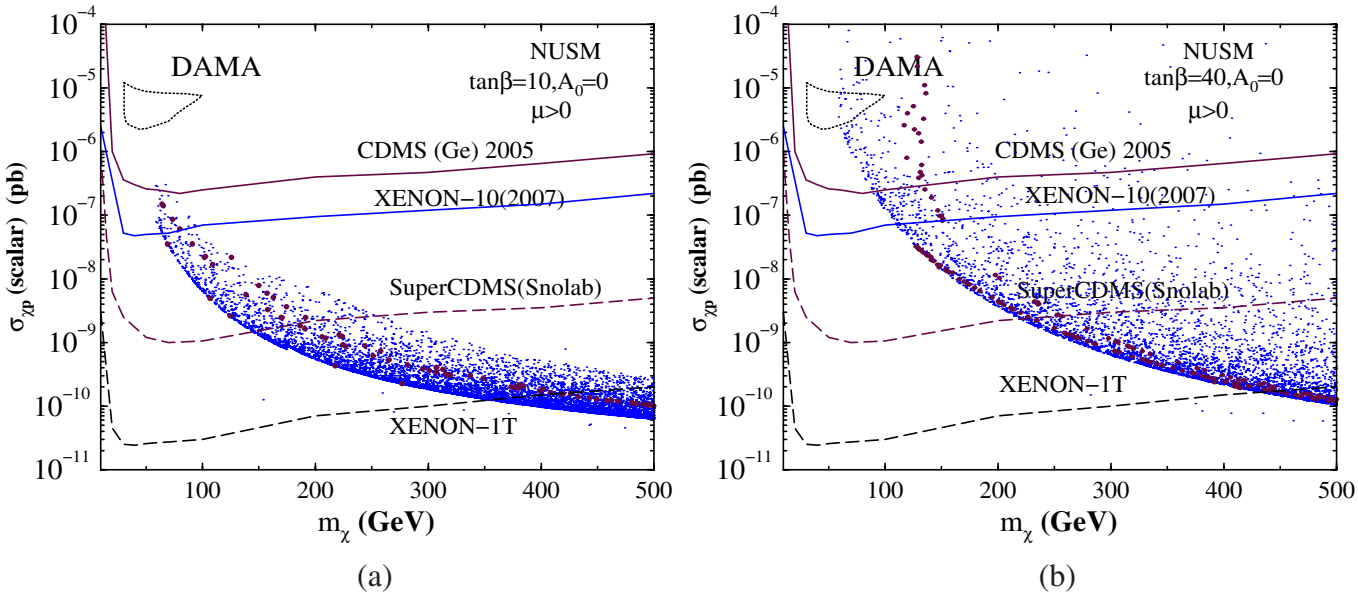

FIG. 6 (color online). Spin-independent scattering LSP-nucleon cross sections vs LSP mass for the NUSM for $\tan\beta = 10$ and 40. The blue dotted region corresponds to scanned points of the parameter space of Figs. 3 and 5. The maroon filled circles show the WMAP allowed points. Various limit plots are shown for different experiments.

B. Indirect detection via photon signal

The fact that the A-resonance annihilation is the primary mechanism to satisfy the WMAP limits in the NUSM suggests that there will be enhanced signals for indirect detection via γ rays, positrons, and antiprotons in the NUSM. On the other hand, detection via the neutrino signal [61] would not be interesting in this case where the LSP is almost a b-ino annihilating via A resonance in the s channel [59]. Among the above indirect detection possibilities we will limit ourselves to estimating only the detection prospect of gamma rays that originates from the galactic center [70–73]. In general for neutralino annihilation at the galactic center one may have the following possibilities: (i) monochromatic γ rays and (ii) continuum γ rays. Monochromatic γ rays come out from processes like $\chi\chi \to \gamma\gamma$ [74] and $\chi\chi \to Z\gamma$ [75]. These signals although small because of the processes being loop suppressed are clean with definite energies $E_\gamma = m_\chi$ and $E_\gamma = m_\chi - m_Z^2/4m_\chi$. Continuum γ rays on the other hand arise from neutralinos annihilating into a variety of standard model particles. The hadronization and production of neutral pions would follow. Typically pion decay, in particular $\pi^0 \to \gamma\gamma$, would produce a huge number of photons with varying energies.

The differential continuum γ-ray flux that arrives from the angular direction ψ with respect to the galactic center is given by [61,71,72],

$$\frac{d\Phi_\gamma}{dE_\gamma}(E_\gamma, \psi) = \sum_i \frac{\langle\sigma_i v\rangle}{8\pi m_\chi^2}\frac{dN_\gamma^i}{dE_\gamma}\int_{\text{line of sight}} ds\rho_\chi^2(r(s,\psi)). \tag{20}$$

Here σ_i is a LSP pair annihilation cross section into a final channel i. We will consider γ rays emerging from the galactic center, hence $\psi = 0$. v is the pair's relative velocity and $\langle\sigma v\rangle$ refers to the velocity averaged value of σv. $\frac{dN_\gamma^i}{dE_\gamma}$ is the differential γ-ray yield for the channel i. $\rho_\chi(r)$ is the cold dark matter density at a distance r from the galactic center, where $r^2 = s^2 + R_0^2 - 2sR_0\cos\psi$. Here, s is the line of sight coordinate, R_0 is the solar distance to the galactic center. Clearly, $\rho_\chi(r)$ that depends on astrophysical modelling is important to determine the photon flux in Eq. (20). One may indeed preferably isolate the right-hand side of Eq. (20) into a part depending on particle physics and a part depending on astrophysics. For the latter, one defines a dimensionless quantity $J(\psi)$ such that

$$J(\psi) = \left(\frac{1}{8.5\text{ kpc}}\right)\left(\frac{1}{0.3\text{ GeV/cm}^3}\right)^2 \times \int_{\text{line of sight}} ds\rho_\chi^2(r(s,\psi)). \tag{21}$$

The above results in

$$\frac{d\Phi_\gamma}{dE_\gamma}(E_\gamma, \psi) = 0.94\times 10^{-13}\text{ cm}^{-2}\text{ s}^{-1}\text{ GeV}^{-1}\text{ sr}^{-1} \times \sum_i \frac{dN_\gamma^i}{dE_\gamma}\left(\frac{\langle\sigma_i v\rangle}{10^{-29}\text{ cm}^3\text{ s}^{-1}}\right) \times \left(\frac{100\text{ GeV}}{m_\chi}\right)^2 J(\psi). \tag{22}$$

For a detector that has an angular acceptance $\Delta\Omega$ and lowest energy threshold of E_{th} the total gamma-ray flux

TABLE II. A few dark matter halo density profiles and associated parameters.

Halo model	a (kpc)	R_0 (kpc)	α	β	γ	$\bar{J}(10^{-3})$	$\bar{J}(10^{-5})$
Isothermal cored	3.5	8.5	2	2	0	30.35	30.4
NFW	20.0	8.0	1	3	1	1.21×10^3	1.26×10^4
Moore	28.0	8.0	1.5	3	1.5	1.05×10^5	9.75×10^6

from the galactic center is given by

$$\Phi_\gamma(E_{\rm th}) = 0.94 \times 10^{-13}\ {\rm cm}^{-2}\,{\rm s}^{-1} \sum_i \int_{E_{\rm th}}^{m_\chi} dE_\gamma \frac{dN_\gamma^i}{dE_\gamma} \times \left(\frac{\langle \sigma_i v\rangle}{10^{-29}\ {\rm cm}^3\,{\rm s}^{-1}}\right)\left(\frac{100\ {\rm GeV}}{m_\chi}\right)^2 \bar{J}(\Delta\Omega)\Delta\Omega. \quad (23)$$

Here $\bar{J}(\Delta\Omega) = \frac{1}{\Delta\Omega}\int_{\Delta\Omega} J(\psi) d\Omega$. The upper limit of the integral in Eq. (23) is fixed by the fact that the neutralinos move with galactic velocity, therefore the annihilations may be considered to have occurred at rest. We will now comment on the galactic halo density profiles used in this analysis. Various N-body simulations suggest that one may obtain a general profile behavior arbitrary to the extent of a

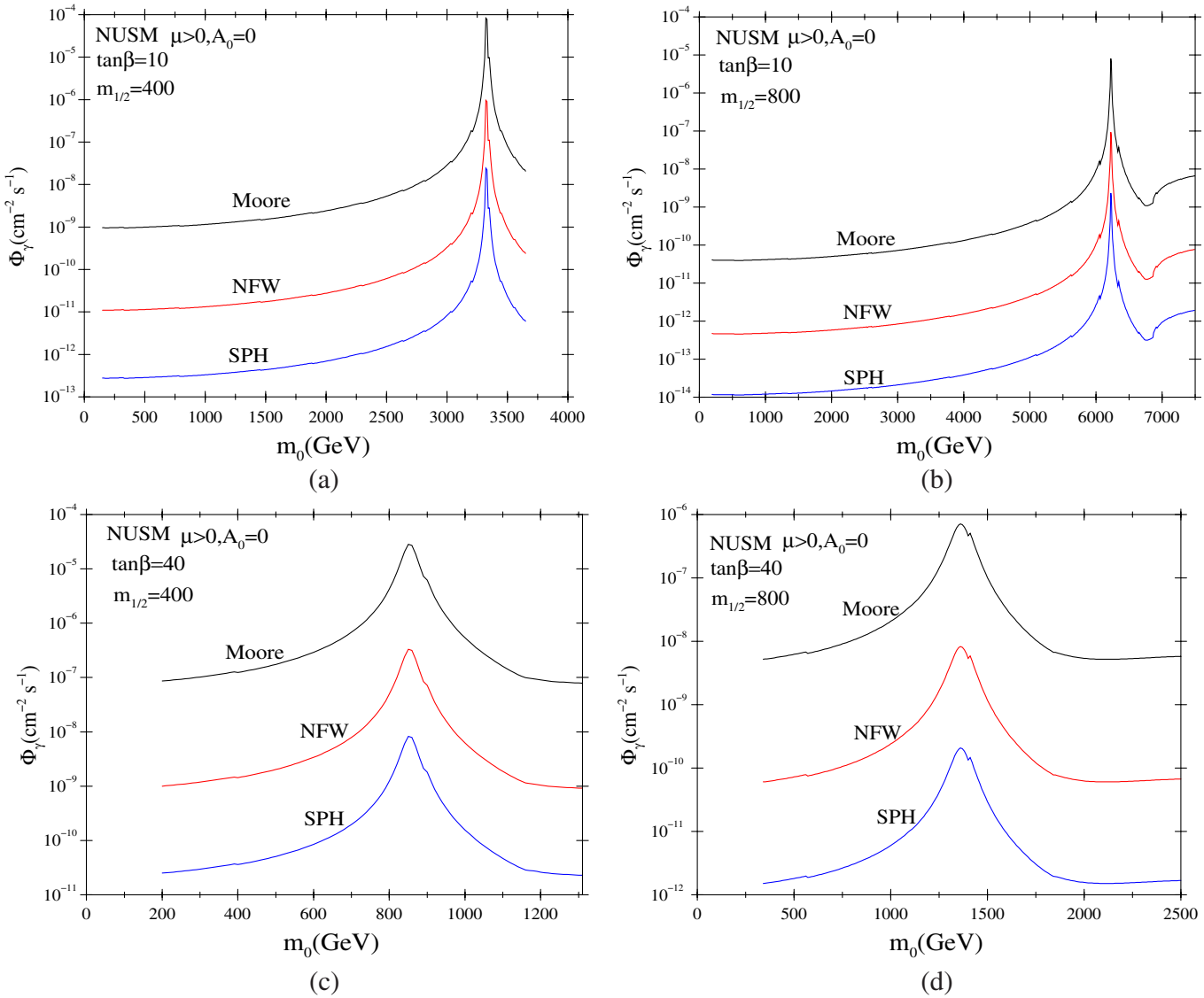

FIG. 7 (color online). Continuous γ-ray flux in ${\rm cm}^{-2}\,{\rm s}^{-1}$ above a threshold energy of 1 GeV for a cone of 1×10^{-3} sr centered around the galactic center vs m_0. Lines are shown for three different halo distributions (i) spherically symmetric isothermal cored profile (SPH) [77], (ii) Navarro, Frenk, and White (NFW) profile [78], and (iii) Moore profile [79].

few parameters and this is given by [76],

$$\rho(r) = \rho_0 \frac{[1 + (R_0/a)^\alpha]^{(\beta-\gamma)/\alpha}}{(r/R_0)^\gamma [1 + (r/a)^\alpha]^{(\beta-\gamma)/\alpha}}. \quad (24)$$

Here ρ_0 is a normalization factor which is taken as the local (i.e. solar region) halo density ($\simeq 0.3$ GeV/cm^3). We will analyze with three popularly used profiles, namely, the isothermal cored [77], Navarro, Frenk, and White (NFW) profile [78], and Moore profile [79] as given in the Table II. The table also mentions the corresponding value of $\bar{J}$ for $\Delta\Omega = 10^{-3}$ and 10^{-5} sr. Computation of the photon flux for a different halo profile may easily be performed by an appropriate scaling with the corresponding $\bar{J}$. Clearly, more cuspy profiles would produce higher photon flux. One can further include the effects of baryons on the dark matter halo profiles. Baryons may undergo radiative processes leading to a fall towards the central region of a galaxy in formation. This changes the density profiles of matter towards the center which in turn leads to an increased concentration of dark matter. Adiabatic compression [80] has been used to study the baryonic effects. Inclusion of adiabatic compression effects cause the profiles to become significantly cuspier, often increasing $\bar{J}$ by a factor of 100 or so [72]. We have not included these halo profile models in our computation, but the photon flux would increase by a similar factor as mentioned above. Figure 7 shows the result of continuum photon flux vs m_0 for $\tan\beta = 10$ and 40 corresponding to two different values of $m_{1/2}$ (= 400 and 800 GeV) and three different halo profiles as mentioned above. The photon flux (in cm^{-2} s^{-1}) in the NUSM is computed using DARKSUSY [65] with $E_\gamma > 1$ GeV, for a solid angle aperture of $\Delta\Omega = 10^{-3}$ sr. As m_0 increases the mass of the psuedoscalar Higgs boson decreases and the LSP pair annihilation through the s-channel resonance causes a peak corresponding to a halo profile. Broadly, such a peak covers the region of m_0 for a given $m_{1/2}$ where WMAP data for the neutralino relic density is satisfied. With an increase in $\tan\beta$ the width Γ_A of m_A increases and the peak associated with a given halo profile broadens. We see that in spite of having a broad range of halo profile characteristics, the photon flux in the region of resonance annihilation in the NUSM where the WMAP data is satisfied may be probed in the upcoming GLAST [81,82] experiment at least for the cuspier profiles. GLAST would be able to probe photon flux as low as 10^{-10} photons/cm^2/s [82]. We note that this conclusion remains valid in spite of the fact that GLAST will use an aperture of $\Delta\Omega = 10^{-5}$ sr so that an appropriate scaling of the photon flux in Fig. 7 needs to be done from Table II and Eq. (23). We further note that as mentioned before, the use of the adiabatic compression mechanism would modify a given halo profile significantly and this may increase the photon flux by a few orders of magnitude. Figure 8 shows the plots of photon flux (in cm^{-2} s^{-1} with $E_\gamma > 1$ GeV) vs the mass of the LSP for $\tan\beta = 10$ and 40 for the NFW halo profile in the NUSM. Here, $m_{1/2}$ and m_0 are varied such that $m_{1/2} < 2$ TeV and $m_0 < 20$ TeV for $\tan\beta = 10$ and $m_{1/2} < 2$ TeV and $m_0 < 10$ TeV for $\tan\beta = 40$. Only WMAP allowed parameter points are shown. GLAST would be able to probe up to 400 to 450 GeV.

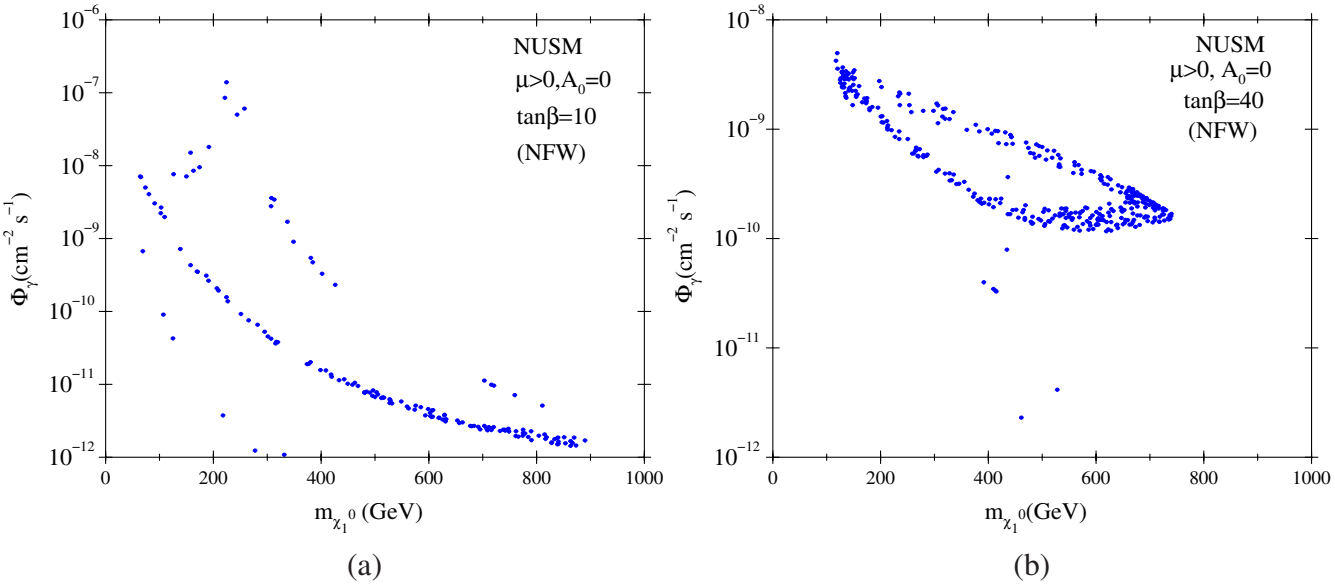

FIG. 8 (color online). Scatter plot of photon flux in cm^{-2} s^{-1} (with $E_\gamma > 1$ GeV) vs LSP mass for $\tan\beta = 10$ and 40 for a NFW halo profile in the NUSM. Here $m_{1/2}$ and m_0 are scanned in the ranges shown in Figs. 3 and 5. Only WMAP relic density satisfied points are shown.

V. CONCLUSION

In this analysis we have worked with a nonuniversal scalar mass scenario in a supergravity framework. We started with purely phenomenological motivations, namely, (i) to manage the FCNC and *CP*-violation type of constraints by decoupling, (ii) to obtain WMAP satisfied values for neutralino relic density for a broad region of parameter space without depending on any delicate mixing of gauginos and Higgsinos, (iii) to have radiative electroweak symmetry breaking, and (iv) to keep naturalness within control. Keeping the above in mind and considering a unified gaugino mass scenario, we used a common scalar mass parameter m_0 at the gauge coupling unification scale for the first two generations of scalars as well as the third generation of sleptons. The item (i) mentioned above would require m_0 to be large, and the item (iv) would prefer a light third generation of squarks and light Higgs scalars. For simplicity we used a vanishing third generation of squarks and Higgs scalar masses at the unification scale. In such a scenario with a possibly multi-TeV m_0, we first found a large mass effect or, in particular, large slepton mass effect in the RGE of $m^2_{H_D}$ (i.e. for the down type of Higgs scalar) that turns the latter negative at the electroweak scale almost irrespective of a value of $\tan\beta$. Extending the semianalytic solution of m^2_A by considering the h_b and the h_τ terms (this is required here even for a small $\tan\beta$) relevant for the large slepton mass effect we found a hyperbolic branch/focus point-like effect in $m^2_A (\simeq m^2_{H_D} - m^2_{H_U})$ for small $\tan\beta$. This causes m_A to be almost independent of m_0 for a large domain of the latter. But, with a very large m_0 this causes m_A to become very light or this may even turn m^2_A negative giving rise to no radiative electroweak symmetry breaking. We further found that because of such a large slepton mass effect in the RGE, the Higgs sector may reach an intense-coupling region with all the Higgs bosons becoming very light and this may evade the LEP2 limit of m_h for a limited region of parameter space. However, the constraint from $\mathrm{Br}(B_s \to \mu^+\mu^-)$ becomes stringent in this region because of lighter m_A. In general, we find relatively lighter m_A or m_H and this fact leads to a large A-pole annihilation region or funnel region of dark matter even for a small $\tan\beta$. This is in contrast to the minimal supergravity type of scenarios where the funnel region may occur only for large values of $\tan\beta$. The nature of the LSP is b-ino dominated, thus there is no need of any delicate mixing of b-inos and Higgsinos in order to satisfy the neutralino relic density constraint. We have also computed the direct detection rates of LSP-nucleon scattering. The upcoming detectors like XENON-1T would be able to probe almost the entire region of parameter space. We have further estimated the indirect detection prospect via computing continuous photon fluxes. The ongoing GLAST experiment will be successfully able to probe the parameter space even for a less cuspy halo profile. We have also briefly discussed the detection prospect of sparticles in the LHC. The Higgs bosons and the third generation of squarks are light in this scenario. In addition to charginos and neutralinos the above may be easily probed in the early runs of the LHC.

ACKNOWLEDGMENTS

D. D. would like to thank the Council of Scientific and Industrial Research, Government of India for support. U. C. is thankful to the organizers of the workshop ''TeV Scale and Dark Matter (2008)'' at NORDITA where the last part of the work was completed. U. C. acknowledges useful discussions with M. Guchait, A. Kundu, B. Mukhopadhyaya, D. Choudhury, D. P. Roy, J. Kalinowski, and S. Roy.

APPENDIX

The coefficients appearing in Eqs. (7) and (8) are given by

$$C_2 = \frac{\tan^2\beta}{(\tan^2\beta - 1)}k,$$
$$C_3 = -\frac{1}{(\tan^2\beta - 1)}(g - e\tan^2\beta), \quad \text{and}$$
$$C_4 = -\frac{\tan^2\beta}{(\tan^2\beta - 1)}f, \tag{A1}$$

$$D_2 = \frac{\tan^2\beta + 1}{\tan^2\beta - 1}k,$$
$$D_3 = -\frac{\tan^2\beta + 1}{\tan^2\beta - 1}(g - e), \quad \text{and}$$
$$D_4 = -\frac{\tan^2\beta + 1}{\tan^2\beta - 1}f. \tag{A2}$$

Here the functions k, g, e, and f may be seen in Ref. [35]. The electroweak scale results of $Y_i = h_i^2/(4\pi)^2$ with $i \equiv t$, b, and τ are shown below:

$$Y_1(t) = \frac{E_1(t)Y_1(0)}{1 + 6Y_1(0)F(t)},$$
$$Y_2(t) = \frac{E_2(t)Y_2(0)}{(1 + 6Y_1(0)F(t))^{1/6}}, \quad \text{and}$$
$$Y_3(t) = Y_3(0)E_3(t). \tag{A3}$$

The quantities $E_i(t)$ are defined as follows:

$$E_1(t) = (1 + \beta_3(t))^{16/3b_3}(1 + \beta_2(t))^{3/b_2}(1 + \beta_1(t))^{13/19b_1},$$
$$E_2(t) = (1 + \beta_1(t))^{(-2)/3b_1}E_1(t),$$
$$E_3(t) = (1 + \beta_1(t))^{3/b_1}(1 + \beta_2(t))^{3/b_2}. \tag{A4}$$

Here, $F(t) = \int_0^t E_1(t')dt'$, $\beta_i = \alpha_i(0)b_i/4\pi$ and $(b_1, b_2, b_3) = (33/5, 1, -3)$.

[1] For reviews on Supersymmetry, see, e.g., H. P. Nilles, Phys. Rep. **110**, 1 (1984); H. E. Haber and G. Kane, Phys. Rep. **117**, 75, 1985); J. Wess and J. Bagger, *Supersymmetry and Supergravity* (Princeton University, Princeton, NJ, 1991), 2nd ed.; M. Drees, P. Roy, and R. M. Godbole, *Theory and Phenomenology of Sparticles* (World Scientific, Singapore, 2005).

[2] T. P. Cheng and L. F. Li (Clarendon, Oxford, 1984, p. 536.

[3] D. J. H. Chung, L. L. Everett, G. L. Kane, S. F. King, J. D. Lykken, and L. T. Wang, Phys. Rep. **407**, 1 (2005); S. P. Martin, arXiv:hep-ph/9709356.

[4] A. H. Chamseddine, R. Arnowitt, and P. Nath, Phys. Rev. Lett. **49**, 970 (1982); R. Barbieri, S. Ferrara, and C. A. Savoy, Phys. Lett. B **119**, 343 (1982); L. J. Hall, J. Lykken, and S. Weinberg, Phys. Rev. D **27**, 2359 (1983); P. Nath, R. Arnowitt, and A. H. Chamseddine, Nucl. Phys. **B227**, 121 (1983); N. Ohta, Prog. Theor. Phys. **70**, 542 (1983); For reviews, see [1] and P. Nath, R. Arnowitt, and A. H. Chamseddine, *Applied* $N = 1$ *Supergravity* (World Scientific, Singapore, 1984).

[5] V. Berezinsky, A. Bottino, J. Ellis, N. Forrengo, G. Mignola, and S. Scopel, Astropart. Phys. **5**, 1 (1996).

[6] P. Nath and R. Arnowitt, Phys. Rev. D**56**, 2820 (1997).

[7] D. G. Cerdeno and C. Munoz, J. High Energy Phys. 10 (2004) 015.

[8] J. Ellis, K. A. Olive, and P. Sandick, Phys. Rev. D**78**, 075012 (2008); J. R. Ellis, K. A. Olive, Y. Santoso, and V. C. Spanos, Phys. Lett. B **603**, 51 (2004); J. R. Ellis, T. Falk, K. A. Olive, and Y. Santoso, Nucl. Phys. **B652**, 259 (2003); A. De Roeck, J. R. Ellis, F. Gianotti, F. Moortgat, K. A. Olive, and L. Pape, Eur. Phys. J. C **49**, 1041 (2007).

[9] H. Baer, A. Mustafayev, E. K. Park, and X. Tata, J. High Energy Phys. 05 (2008) 058; H. Baer, A. Mustafayev, E. K. Park, S. Profumo, and X. Tata, J. High Energy Phys. 04 (2006) 041; S. Bhattacharya, A. Datta, and B. Mukhopadhyaya, arXiv:0804.4051; Phys. Rev. D **78**, 115018 (2008).

[10] H. Baer, A. Mustafayev, S. Profumo, A. Belyaev, and X. Tata, J. High Energy Phys. 07 (2005) 065; Phys. Rev. D **71**, 095008 (2005).

[11] U. Chattopadhyay, D. Choudhury, and D. Das, Phys. Rev. D **72**, 095015 (2005); U. Chattopadhyay and D. P. Roy, Phys. Rev. D **68**, 033010 (2003); A. Corsetti and P. Nath, Phys. Rev. D **64**, 125010 (2001); U. Chattopadhyay, A. Corsetti, and P. Nath, Phys. Rev. D **66**, 035003 (2002); U. Chattopadhyay and P. Nath, Phys. Rev. D **65**, 075009 (2002); S. Bhattacharya, A. Datta, and B. Mukhopadhyaya, J. High Energy Phys. 10 (2007) 080; Phys. Rev. D **78**, 035011 (2008); K. Huitu, J. Laamanen, P. N. Pandita, and S. Roy, Phys. Rev. D **72**, 055013 (2005); K. Huitu, R. Kinnunen, J. Laamanen, S. Lehti, S. Roy, and T. Salminen, Eur. Phys. J. C **58**, 591 (2008); S. F. King, J. P. Roberts, and D. P. Roy, J. High Energy Phys. 10 (2007) 106; G. Belanger, F. Boudjema, A. Cottrant, A. Pukhov, and A. Semenov, Nucl. Phys. **B706**, 411 (2005).

[12] S. K. Soni and H. A. Weldon, Phys. Lett. B **126**, 215 (1983); V. S. Kaplunovsky and J. Louis, Phys. Lett. B **306**, 269 (1993).

[13] M. Dine, R. Leigh, and A. Kagan, Phys. Rev. D **48**, 4269 (1993); P. Pouliot and N. Seiberg, Phys. Lett. B **318**, 169 (1993); Y. Nir and N. Seiberg, Phys. Lett. B **309**, 337 (1993); S. Dimopoulos and G. F. Giudice, Phys. Lett. B **357**, 573 (1995); A. Cohen, D. B. Kaplan, and A. E. Nelson, Phys. Lett. B **388**, 588 (1996); M. Misiak, S. Pokorski, and J. Rosiek, Adv. Ser. Dir. High Energy Phys. **15**, 795 (1998); P. H. Chankowski, K. Kowalska, S. Lavignac, and S. Pokorski, arXiv:hep-ph/0507133.

[14] N. Arkani-Hamed and H. Murayama, Phys. Rev. D **56**, R6733 (1997).

[15] F. Gabbiani, E. Gabrielli, A. Masiero, and L. Silvestrini, Nucl. Phys. **B477**, 321 (1996).

[16] R. Barbieri and G. F. Giudice, Nucl. Phys. **B306**, 63 (1988); P. Ciafaloni and A. Strumia, Nucl. Phys. **B494**, 41 (1997); G. Bhattacharya and A. Romanino, Phys. Rev. D **55**, 7015 (1997).

[17] J. Bagger, J. L. Feng, and N. Polonsky, Nucl. Phys. **B563**, 3 (1999); K. Agashe and M. Graesser, Phys. Rev. D **59**, 015007 (1998); J. A. Bagger, J. L. Feng, N. Polonsky, and R. J. Zhang, Phys. Lett. B **473**, 264 (2000).

[18] H. Baer, C. Balazs, P. Mercadante, X. Tata, and Y. Wang, Phys. Rev. D **63**, 015011 (2000).

[19] J. L. Feng, K. T. Matchev, and T. Moroi, Phys. Rev. D **61**, 075005 (2000); Phys. Rev. Lett. **84**, 2322 (2000); J. L. Feng, K. T. Matchev, and F. Wilczek, Phys. Lett. B **482**, 388 (2000); J. L. Feng and F. Wilczek, Phys. Lett. B **631**, 170 (2005); U. Chattopadhyay, T. Ibrahim, and D. P. Roy, Phys. Rev. D **64**, 013004 (2001); U. Chattopadhyay, A. Datta, A. Datta, A. Datta, and D. P. Roy, Phys. Lett. B **493**, 127 (2000); S. P. Das, A. Datta, M. Guchait, M. Maity, and S. Mukherjee, Eur. Phys. J. C **54**, 645 (2008).

[20] K. L. Chan, U. Chattopadhyay, and P. Nath, Phys. Rev. D **58**, 096004 (1998); U. Chattopadhyay, A. Corsetti, and P. Nath, Phys. Rev. D **68**, 035005 (2003); See also: first article of Ref. [39].

[21] V. D. Barger, C. Kao, and R. J. Zhang, Phys. Lett. B **483**, 184 (2000).

[22] H. Baer, A. Belyaev, T. Krupovnickas, and A. Mustafayev, J. High Energy Phys. 06 (2004) 044.

[23] S. F. King and J. P. Roberts, J. High Energy Phys. 09 (2006) 036.

[24] D. G. Cerdeno, S. Khalil, and C. Munoz, arXiv:hep-ph/0105180.

[25] N. Arkani-Hamed, A. Delgado, and G. F. Giudice, Nucl. Phys. **B741**, 108 (2006).

[26] C. D. McMullen and S. Nandi, Phys. Rev. D **75**, 095001 (2007).

[27] D. Feldman, Z. Liu, and P. Nath, J. High Energy Phys. 04 (2008) 054; Phys. Rev. Lett. **99**, 251802 (2007); **100**, 069902(E) (2008).

[28] L. Randall and R. Sundrum, Nucl. Phys. **B557**, 79 (1999); G. F. Giudice, M. A. Luty, H. Murayama, and R. Rattazzi, J. High Energy Phys. 12 (1998) 027; T. Gherghetta, G. F. Giudice, and J. D. Wells, Nucl. Phys. **B559**, 27 (1999).

[29] A. Brignole, L. E. Ibanez, and C. Munoz, Nucl. Phys. **B422**, 125 (1994); **B436**, 747(E) (1995); L. E. Ibanez, D. Lust, and G. G. Ross, Phys. Lett. B **272**, 251 (1991).

[30] D. G. Cerdeno, T. Kobayashi, and C. Munoz, J. High Energy Phys. 01 (2008) 009.

[31] H. E. Haber and Y. Nir, Phys. Lett. B **306**, 327 (1993); H. E. Haber, arXiv:hep-ph/9505240; A. Dobado, M. J. Herrero, and S. Penaranda, Eur. Phys. J. C **17**, 487 (2000); J. F. Gunion and H. E. Haber, Phys. Rev. D **67**,

075019 (2003).
[32] A. Djouadi and Y. Mambrini, J. High Energy Phys. 12 (2006) 001; E. Boos, V. Bunichev, A. Djouadi, and H. J. Schreiber, Phys. Lett. B **622**, 311 (2005); E. Boos, A. Djouadi, and A. Nikitenko, Phys. Lett. B **578**, 384 (2004); E. Boos, A. Djouadi, M. Muhlleitner, and A. Vologdin, Phys. Rev. D **66**, 055004 (2002).
[33] R. Arnowitt and P. Nath, Phys. Rev. D **46**, 3981 (1992).
[34] G. Gamberini, G. Ridolfi, and F. Zwirner, Nucl. Phys. **B331**, 331 (1990); V. D. Barger, M. S. Berger, and P. Ohmann, Phys. Rev. D **49**, 4908 (1994); For two-loop effective potential see: S. P. Martin, Phys. Rev. D **66**, 096001 (2002).
[35] L. E. Ibanez, C. Lopez, and C. Munoz, Nucl. Phys. **B256**, 218 (1985); L. E. Ibanez and C. Lopez, Nucl. Phys. **B233**, 511 (1984).
[36] A. Djouadi, J. L. Kneur, and G. Moultaka, Comput. Phys. Commun. **176**, 426 (2007).
[37] J. R. Ellis, K. A. Olive, and P. Sandick, Phys. Lett. B **642**, 389 (2006).
[38] G. Jungman, M. Kamionkowski, and K. Greist, Phys. Rep. **267**, 195 (1996).
[39] A. B. Lahanas, N. E. Mavromatos, and D. V. Nanopoulos, Int. J. Mod. Phys. D **12**, 1529 (2003); C. Munoz, Int. J. Mod. Phys. A **19**, 3093 (2004); M. Drees, Plenary talk at *11th International Symposium on Particles, Strings and Cosmology (PASCOS 2005), Gyeongju, Korea, 2005*, AIP Conf. Proc. (AIP, New York, 2006), Vol. 805, p. 48.
[40] E. Komatsu *et al.* (WMAP Collaboration), arXiv:0803.0547.
[41] J. R. Ellis, T. Falk, and K. A. Olive, Phys. Lett. B **444**, 367 (1998); J. R. Ellis, T. Falk, K. A. Olive, and M. Srednicki, Astropart. Phys. **13**, 181 (2000); **15**, 413(E) (2001); A. Lahanas, D. V. Nanopoulos, and V. Spanos, Phys. Rev. D **62**, 023515 (2000); R. Arnowitt, B. Dutta, and Y. Santoso, Nucl. Phys. **B606**, 59 (2001); T. Nihei, L. Roszkowski, and R. Ruiz de Austri, J. High Energy Phys. 07 (2002) 024; V. A. Bednyakov, H. V. Klapdor-Kleingrothaus, and V. Gronewold, Phys. Rev. D **66**, 115005 (2002).
[42] C. Boehm, A. Djouadi, and M. Drees, Phys. Rev. D **62**, 035012 (2000); J. R. Ellis, K. A. Olive, and Y. Santoso, Astropart. Phys. **18**, 395 (2003); See also Ref. [48].
[43] J. Edsjo and P. Gondolo, Phys. Rev. D **56**, 1879 (1997).
[44] S. Mizuta and M. Yamaguchi, Phys. Lett. B **298**, 120 (1993).
[45] R. Arnowitt, B. Dutta, and Y. Santoso, Nucl. Phys. **B606**, 59 (2001); V. A. Bednyakov, H. V. Klapdor-Kleingrothaus, and V. Gronewold, Phys. Rev. D **66**, 115005 (2002).
[46] For the latest limits on the sparticle masses from LEP experiments: see http://lepsusy.web.cern.ch/lepsusy/.
[47] R. Barate *et al.* (LEP Working Group for Higgs boson searches), Phys. Lett. B **565**, 61 (2003).
[48] U. Chattopadhyay, D. Das, A. Datta, and S. Poddar, Phys. Rev. D **76**, 055008 (2007); N. Bhattacharyya, A. Datta, and S. Poddar, Phys. Rev. D **78**, 075030 (2008).
[49] M. Drees and M. Nojiri, Phys. Rev. D **47**, 376 (1993).
[50] R. Arnowitt and P. Nath, Phys. Rev. Lett. **70**, 3696 (1993); H. Baer and M. Brhlik, Phys. Rev. D **53**, 597 (1996); **57**, 567 (1998); H. Baer, M. Brhlik, M. Diaz, J. Ferrandis, P. Mercadante, P. Quintana, and X. Tata, Phys. Rev. D **63**, 015007 (2000); J. R. Ellis, T. Falk, G. Ganis, K. A. Olive, and M. Srednicki, Phys. Lett. B **510**, 236 (2001); A. B. Lahanas and V. C. Spanos, Eur. Phys. J. C **23**, 185 (2002); A. Djouadi, M. Drees, and J. Kneur, Phys. Lett. B **624**, 60 (2005).
[51] G. Belanger, F. Boudjema, A. Pukhov, and A. Semenov, Comput. Phys. Commun. **176**, 367 (2007).
[52] J. M. Frere, D. R. T. Jones, and S. Raby, Nucl. Phys. **B222**, 11 (1983); J. A. Casas, A. Lleyda, and C. Munoz, Nucl. Phys. **B471**, 3 (1996).
[53] S. Heinemeyer, W. Hollik, and G. Weiglein, Phys. Rep. **425**, 265 (2006); S. Heinemeyer, arXiv:hep-ph/0408340; S. Heinemeyer, Int. J. Mod. Phys. A **21**, 2659 (2006); G. Degrassi, S. Heinemeyer, W. Hollik, P. Slavich, and G. Weiglein, Eur. Phys. J. C **28**, 133 (2003); B. C. Allanach, A. Djouadi, J. L. Kneur, W. Porod, and P. Slavich, J. High Energy Phys. 09 (2004) 044.
[54] S. Chen *et al.* (CLEO Collaboration), Phys. Rev. Lett. **87**, 251807 (2001); P. Koppenburg *et al.* (Belle Collaboration), Phys. Rev. Lett. **93**, 061803 (2004); B. Aubert *et al.* (*BABAR* Collaboration), arXiv:hep-ex/0207076.
[55] K. i. Okumura and L. Roszkowski, Phys. Rev. Lett. **92**, 161801 (2004); M. E. Gomez, T. Ibrahim, P. Nath, and S. Skadhauge, Phys. Rev. D **74**, 015015 (2006).
[56] A. Djouadi, M. Drees, and J. L. Kneur, J. High Energy Phys. 03 (2006) 033.
[57] T. Aaltonen *et al.* (CDF Collaboration), Phys. Rev. Lett. **100**, 101802 (2008).
[58] J. R. Ellis, K. A. Olive, and V. C. Spanos, Phys. Lett. B **624**, 47 (2005); T. Ibrahim and P. Nath, Phys. Rev. D **67**, 016005 (2003); S. Baek, P. Ko, and W. Y. Song, J. High Energy Phys. 03 (2003) 054; J. K. Mizukoshi, X. Tata, and Y. Wang, Phys. Rev. D **66**, 115003 (2002); R. Arnowitt, B. Dutta, T. Kamon, and M. Tanaka, Phys. Lett. B **538**, 121 (2002); A. Dedes, H. K. Dreiner, U. Nierste, and P. Richardson, Phys. Rev. Lett. **87**, 251804 (2001); K. S. Babu and C. Kolda, Phys. Rev. Lett. **84**, 228 (2000); S. R. Choudhury and N. Gaur, Phys. Lett. B **451**, 86 (1999).
[59] H. Baer, A. Belyaev, T. Krupovnickas, and J. O'Farrill, J. Cosmol. Astropart. Phys. 08 (2004) 005; H. Baer and J. O'Farrill, J. Cosmol. Astropart. Phys. 04 (2004) 005.
[60] M. Passera, W. J. Marciano, and A. Sirlin, Phys. Rev. D **78**, 013009 (2008).
[61] G. Bertone, D. Hooper, and J. Silk, Phys. Rep. **405**, 279 (2005); G. Bertone and D. Merritt, Mod. Phys. Lett. A **20**, 1021 (2005); J. Carr, G. Lamanna, and J. Lavalle, Rep. Prog. Phys. **69**, 2475 (2006).
[62] M. W. Goodman and E. Witten, Phys. Rev. D **31**, 3059 (1985); K. Greist, Phys. Rev. D **38**, 2357 (1988); J. Ellis and R. Flores, Nucl. Phys. **B307**, 883 (1988); R. Barbieri, M. Frigeni, and G. Giudice, Nucl. Phys. **B313**, 725 (1989); A. Bottino *et al.*, Phys. Lett. B **295**, 330 (1992); M. Drees and M. M. Nojiri, Phys. Rev. D **48**, 3483 (1993); J. R. Ellis, A. Ferstl, and K. A. Olive, Phys. Lett. B **481**, 304 (2000); J. D. Vergados, Lect. Notes Phys. **720**, 69 (2007); V. K. Oikonomou, J. D. Vergados, and C. C. Moustakidis, Nucl. Phys. **B773**, 19 (2007); J. Ellis, K. A. Olive, and C. Savage, Phys. Rev. D **77**, 065026 (2008); D. Feldman, Z. Liu, and P. Nath, Phys. Lett. B **662**, 190 (2008); Phys. Rev. D **78**, 083523 (2008).

[63] M. Drees and M. Nojiri, Phys. Rev. D **47**, 4226 (1993); **48**, 3483 (1993); M. A. Shifman, A. I. Vainshtein, and V. I. Zakharov, Phys. Lett. B **78**, 443 (1978); A. I. Vainshtein, V. I. Zakharov, and M. A. Shifman, Usp. Fiz. Nauk **131**, 537 (1980).

[64] V. A. Bednyakov, H. V. Klapdor-Kleingrothaus, and S. Kovalenko, Phys. Rev. D **50**, 7128 (1994).

[65] P. Gondolo, J. Edsjo, P. Ullio, L. Bergstrom, M. Schelke, and E. A. Baltz, J. Cosmol. Astropart. Phys. 07 (2004) 008.

[66] D. S. Akerib *et al.* (CDMS Collaboration), Phys. Rev. Lett. **96**, 011302 (2006).

[67] J. Angle *et al.* (XENON Collaboration), Phys. Rev. Lett. **100**, 021303 (2008).

[68] http://www.fermilabtoday.com/directorate/program_planning/March2007PACPublic/CabreraPAC03_07.pdf; For a limit plot see: http://dendera.berkeley.edu/plotter/entryform.html.

[69] http://www.lngs.infn.it/lngs_infn/contents/lngs_en/research/experiments_scientific_info/experiments/current/xenon/collaboration.htm; For a limit plot see: http://dendera.berkeley.edu/plotter/entryform.html.

[70] A. Bouquet, P. Salati, and J. Silk, Phys. Rev. D **40**, 3168 (1989); F. W. Stecker, Phys. Lett. B **201**, 529 (1988); M. Urban, A. Bouquet, B. Degrange, P. Fleury, J. Kaplan, A. L. Melchior, and E. Pare, Phys. Lett. B **293**, 149 (1992); V. S. Berezinsky, A. V. Gurevich, and K. P. Zybin, Phys. Lett. B **294**, 221 (1992); V. Berezinsky, A. Bottino, and G. Mignola, Phys. Lett. B **325**, 136 (1994); G. Bertone, G. Sigl, and J. Silk, Mon. Not. R. Astron. Soc. **337**, 98 (2002); T. Bringmann, L. Bergstrom, and J. Edsjo, J. High Energy Phys. 01 (2008) 049.

[71] L. Bergstrom, P. Ullio, and J. H. Buckley, Astropart. Phys. **9**, 137 (1998).

[72] Y. Mambrini, C. Munoz, E. Nezri, and F. Prada, J. Cosmol. Astropart. Phys. 01 (2006) 010; Y. Mambrini, C. Munoz, and E. Nezri, J. Cosmol. Astropart. Phys. 12 (2006) 003; L. Roszkowski, R. R. de Austri, J. Silk, and R. Trotta, Phys. Lett. B **671**, 10 (2009); S. Profumo and A. Provenza, J. Cosmol. Astropart. Phys. 12 (2006) 019; H. Baer, A. Mustafayev, E. K. Park, and S. Profumo, J. High Energy Phys. 07 (2005) 046.

[73] S. Dodelson, D. Hooper, and P. D. Serpico, Phys. Rev. D **77**, 063512 (2008); D. Hooper, G. Zaharijas, D. P. Finkbeiner, and G. Dobler, Phys. Rev. D **77**, 043511 (2008); D. Hooper and E. A. Baltz, Annu. Rev. Nucl. Part. Sci. **58**, 293 (2008); N. Bernal, A. Goudelis, Y. Mambrini, and C. Munoz, arXiv:0804.1976; A. Birkedal, K. T. Matchev, M. Perelstein, and A. Spray, arXiv:hep-ph/0507194.

[74] L. Bergstrom and P. Ullio, Nucl. Phys. **B504**, 27 (1997); Z. Bern, P. Gondolo, and M. Perelstein, Phys. Lett. B **411**, 86 (1997); U. Chattopadhyay, D. Das, P. Konar, and D. P. Roy, Phys. Rev. D **75**, 073014 (2007); U. Chattopadhyay, D. Choudhury, M. Drees, P. Konar, and D. P. Roy, Phys. Lett. B **632**, 114 (2006).

[75] P. Ullio and L. Bergstrom, Phys. Rev. D **57**, 1962 (1998).

[76] L. Hernquist, Astrophys. J. **356**, 359 (1990).

[77] J. Binney and S. Tremaine, *Galactic Dynamics* (Princeton University Press, Princeton, 1987).

[78] J. F. Navarro, C. S. Frenk, and S. D. M. White, Astrophys. J. **462**, 563 (1996); J. F. Navarro, C. S. Frenk, and S. D. M. White, Astrophys. J. **490**, 493 (1997).

[79] B. Moore, T. Quinn, F. Governato, J. Stadel, and G. Lake, Mon. Not. R. Astron. Soc. **310**, 1147 (1999).

[80] G. R. Blumenthal, S. M. Faber, R. Flores, and J. R. Primack, Astrophys. J. **301**, 27 (1986); R. Jesseit, T. Naab, and A. Burkert, Astrophys. J. Lett. **571**, L89 (2002); O. Y. Gnedin, A. V. Kravtsov, A. A. Klypin, and D. Nagai, Astrophys. J. **616**, 16 (2004); F. Prada, A. Klypin, J. Flix, M. Martinez, and E. Simonneau, Phys. Rev. Lett. **93**, 241301 (2004).

[81] The gamma-ray large area space telescope (GLAST): http://glast.gsfc.nasa.gov.

[82] A. Morselli, A. Lionetto, A. Cesarini, F. Fucito, and P. Ullio (GLAST Collaboration), Nucl. Phys. B, Proc. Suppl. **113**, 213 (2002).